Electronic Supplementary Information

Noble Metal-P-Block-Element Intermetallics with d-p Orbital Hybridization for Highly Efficient Electrocatalysis

Caihong He,‡[ab] Chaoqun Ma,‡[ab] Qinbai Yun,‡[c] Jing Xia,*[d] Sumei Han,[ab] Huaifang Zhang,[ab] Xiao Ma,[ab] Fukai Feng,[ab] Gang Lin,[ab] Jianing Song,[ab] Bin Li,[a] Lijie Zhu,*[e] An-Liang Wang,[f] Xiangmin Meng,[d] Wenbin Cao,[a] Qipeng Lu *[abg]

[a] State Key Laboratory of Nuclear Power Safety Technology and Equipment, University of Science and Technology Beijing, Beijing, 100083, China

[b] School of Materials Science and Engineering, University of Science and Technology Beijing, Beijing 100083, China

[c] Department of Chemical and Biological Engineering & Energy Institute, The Hong Kong University of Science and Technology, Hong Kong, China

[d] Key Laboratory of Photochemical Conversion and Optoelectronic Materials, Technical Institute of Physics and Chemistry, Chinese Academy of Sciences, Beijing 100190, China

[e] School of Instrument Science and Opto-Electronics Engineering, Beijing Information Science and Technology University, Beijing 100192, China.

[f] School of Chemistry and Chemical Engineering, Shandong University, Jinan 250100, China

[g] Shunde Innovation School, University of Science and Technology Beijing, Foshan 528399, China

‡These authors contributed equally to this work.

*Corresponding author. Email: xiajing@mail.ipc.ac.cn; ljzhu@bistu.edu.cn; qipeng@ustb.edu.cn;

Experimental section

Reagents and Chemicals. Iridium (III) chloride hydrate ($IrCl_3 \cdot xH_2O$), tin(II) chloride dihydrate ($SnCl_2 \cdot 2H_2O$), silver nitrate ($AgNO_3$), ruthenium chloride hydrate ($RuCl_3 \cdot xH_2O$), gold chloride trihydrate ($HAuCl_4 \cdot 3H_2O$), potassium tetrachloropalladate (II) (K_2PdCl_4) and chloroplatinic acid hexahydrate ($H_2PtCl_6 \cdot 6H_2O$) are bought from Aladdin Co., Ltd (Shanghai, China). Indium nitrate hydrate ($In(NO_3)_3 \cdot xH_2O$) and cyanamide (CH_2N_2) are purchased from Macklin Biochemical Co., Ltd (Shanghai, China). Ketjen Black EC300J is purchased from Suzhou Sinero Technology co., Ltd. All chemicals are used as received without further purification. Deionized water (18 MΩ cm^{-1}) used for the whole experiment is obtained by reverse osmosis pure water equipment (Sihai Water Treatment Equipment Co., Ltd., Shandong, China).

Material synthesis

Synthesis of Sn and In-based noble metal IMCs supported on commercial carbon. A mixture of noble metal precursors, p-block elemental precursors and 0.06 g of carbon support (Ketjen Black EC300J) is ground using an agate mortar and pestle. The molar ratios of the noble metals and p-block element precursors are stoichiometric moles except for Ir_3Sn_7/C with a mole ratio of 1:2. The sample is sufficiently ground under ambient conditions, directly transferred to a porcelain boat and placed in a tube furnace. It is subsequently heated to 900 °C at a rate of 5 °C min^{-1} under a flowing H_2/Ar (5 vol.% H_2) atmosphere and held at this temperature for 12 h, followed by cooling down to room temperature. The prepared product is treated with 0.5 M H_2SO_4 at room temperature to remove the oxides.

Synthesis of Ir/C. Ir/C is prepared using the same method as Ir_3Sn_7/C, but without adding $SnCl_2 \cdot 2H_2O$.

Synthesis of Sn/C. Sn/C is synthesized using the same method as Ir_3Sn_7/C, but without adding $IrCl_3 \cdot xH_2O$.

Physicochemical characterizations

X-ray powder diffraction (XRD) patterns are collected on a Bruker D8 X-ray diffractometer operating at 40 kV and 40 mA with Cu Kα radiation (λ = 0.154 nm). The patterns of all the samples are analyzed to 2θ ranging from 10° to 90° at a scan rate of 5° min^{-1}. For atomic-level characterization of the Ir_3Sn_7/C, aberration-corrected HAADF-STEM images, elemental mapping images as well as energy-dispersive X-ray spectroscopy (EDS) are performed by using an aberration-corrected JEOL JEM-ARM300F Grand ARM transmission electron microscope operated at 300 kV accelerating voltage equipped with a cold field-emission electron gun and SDD-type EDX detectors. Transmission electron microscopy (TEM) images and selected area electron diffraction (SAED) patterns are obtained using JEOL JEM-2100F transmission electron microscopy at a voltage of 200 kV. Thermogravimetric analysis (TGA) is implemented on a Netzsch STA449C thermal analyzer under a flowing air atmosphere with a heating rate of 10 °C min^{-1}. For the Ir_3Sn_7/C and Ir/C catalysts, the TGA is carried out at 800 °C in the air to burn off the carbon and form a mixture of IrO_2 and SnO_2, which are characterized by using XRD. The TGA and XRD results are used to determine the Ir content of the catalysts. The X-ray photoelectron spectroscopy (XPS) analyses with Al Kα radiation source are acquired using on a Thermo Scientific ESCALAB 250Xi spectrometer. And the C 1s value is set at 284.8 eV for calibration. X-ray absorption spectroscopy (XAS) experiments are performed at the BL14W1 station at the Shanghai Synchrotron Radiation Facility (SSRF) in China. Quantitative analysis of metal contents is conducted by inductively coupled plasma mass spectrometry (ICP-MS) on an Agilent 7800.

Electrochemical measurements

The preparation of the working electrode. The hydrogen evolution reaction (HER) and oxygen evolution reaction (OER) measurements are conducted using a three-electrode cell system with a glassy carbon electrode (GCE) (diameter: 3 mm; area: 0.0706 cm^2) as the working electrode,

a saturated calomel electrode (SCE) as the reference electrode, and a graphite rod as the counter electrode.

To prepare the working electrode, the inks of different electrocatalysts are prepared by sonicating the mixture of a certain amount of the catalyst powder with 950 μL ethanol and 50 μL Nafion for 2 h. Then 10 μL of ink is dropped onto a cleaned GCE and dried naturally. The loading of metal (Ir or Pt) on the working electrode is 5.0 μg for both HER and OER.

Linear-sweep voltammograms measurements are carried out to study the catalytic activity. HER and OER polarization curves are recorded at a scan rate of 5 mV s^{-1} with manually 90% *iR*-corrected after the activation process of catalysts in 1.0 M KOH and 0.5 M H_2SO_4 solutions, respectively. Cyclic voltammogram (CV) curves are conducted with different rates from 20 to 120 mV s^{-1} in the non-Faraday potential region to determine double-layer capacitance. The electrochemical impedance spectroscopy (EIS) measurements are performed with a frequency range from 100 kHz to 0.01 Hz. The potential cycling stability test for HER is examined by taking continuous CVs at a sweep rate of 100 mV s^{-1} over a potential range of -0.2 to 0.0 V for 10,000 cycles. Similarly, the stability of OER is examined at a potential range of 1.4 to 1.6 V, using a sweep rate of 100 mV s^{-1} for 5,000 cycles.

Electrocatalytic overall water splitting performances. For overall water splitting, the measurements are performed in a two-electrode system. Ir_3Sn_7/C modified carbon paper with a geometric area of 1 cm × 1 cm is used as both cathode and anode (Ir_3Sn_7/C||Ir_3Sn_7/C). The polarization curves are measured in different electrolytes (i.e., 1.0 M KOH, 0.5 M H_2SO_4) at a scan rate of 5 mV s^{-1}. Commercial Pt/C || IrO_2 couple is measured for comparison. The long-term durability of overall water splitting is measured by using the chronopotentiometry method (CP), recording at 10 mA cm^{-2} in 1.0 M KOH solutions. All recorded related potentials are transformed to the reversible hydrogen electrode (RHE) according to the following formula: $E_{RHE} = E_{SCE} + 0.059\ pH + 0.241$.

Anion exchange membrane (AEM) water electrolyzer tests. Ir_3Sn_7/C ink is dropped onto carbon paper to form the cathode and anode, respectively. The cathode and the anode were sandwiched with an anion exchange membrane (Fumasep FAA-3-50) to form the membrane electrode assembly (MEA). The polarization curve and stability test were performed in a flowing 1.0 M KOH at 50 °C.

Calculational methods and details

Density functional theory (DFT) calculations are carried out by the Vienna *ab-initio* Simulation Package (VASP) software, using the Perdew-Burke-Ernzerhof (PBE) and generalized gradient approximation (GGA) exchange-correlation function.[1-4] The projector augmented wave (PAW) method is used for the ion-electron interaction.[5] Additionally, the DFT-D3 method is employed for model van der Waals force correction. A plane-wave cutoff energy basis is set to 500 eV, and a Monkhorst-Pack k-point mesh with dimensions of 3×3×1 is utilized during the structure optimization process for all samples.[6, 7] The energy difference within 10^{-5} eV and a force convergence threshold of 0.05 eV $Å^{-1}$ are chosen. Additionally, all periodic slabs have a vacuum layer of at least 15 Å.

The surface energy of Ir_3Sn_7 IMCs can be computed using the following Equation (1).

$$\Delta E_{\text{surface}} = (E_{\text{surface}} - E_{\text{bulk}})/2A \quad (1)$$

In this equation, $\Delta E_{\text{surface}}$, E_{surface}, E_{bulk} and A represent the theoretical surface energy, total energy of the surface model in VASP, energy of each atom in the bulk model and surface area, respectively.[8]

The free energy change (ΔG) of each elementary reaction can be computed by the following Equation (2):

$$\Delta G = \Delta E + \Delta ZPE - T\Delta S \quad (2)$$

In this equation, ΔE, ΔZPE, T and ΔS represent reaction energy difference, zero-point energy change, temperature, and entropy change, respectively

Supporting Figures

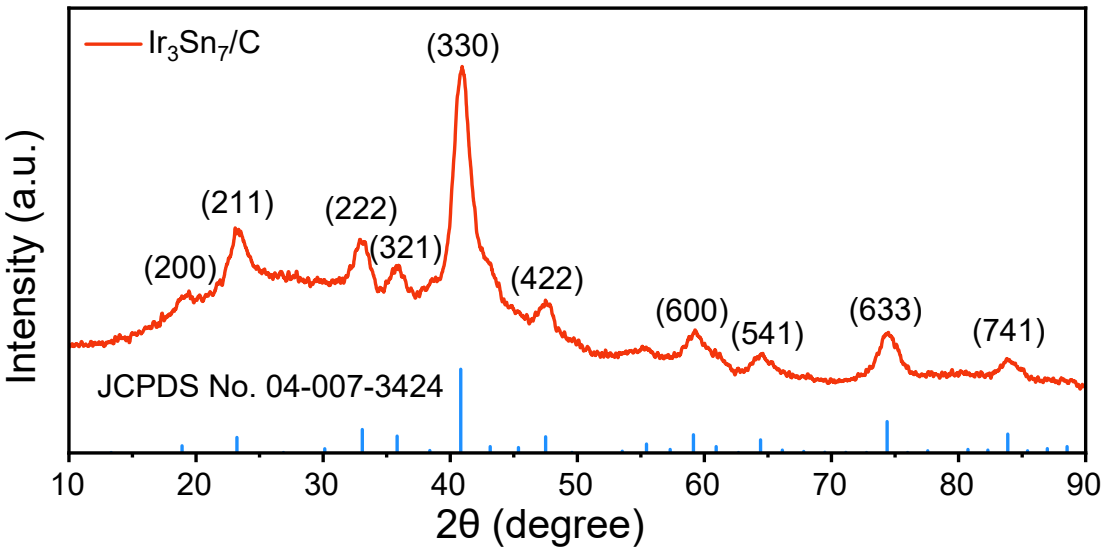

Fig. S1. XRD pattern of Ir_3Sn_7/C.

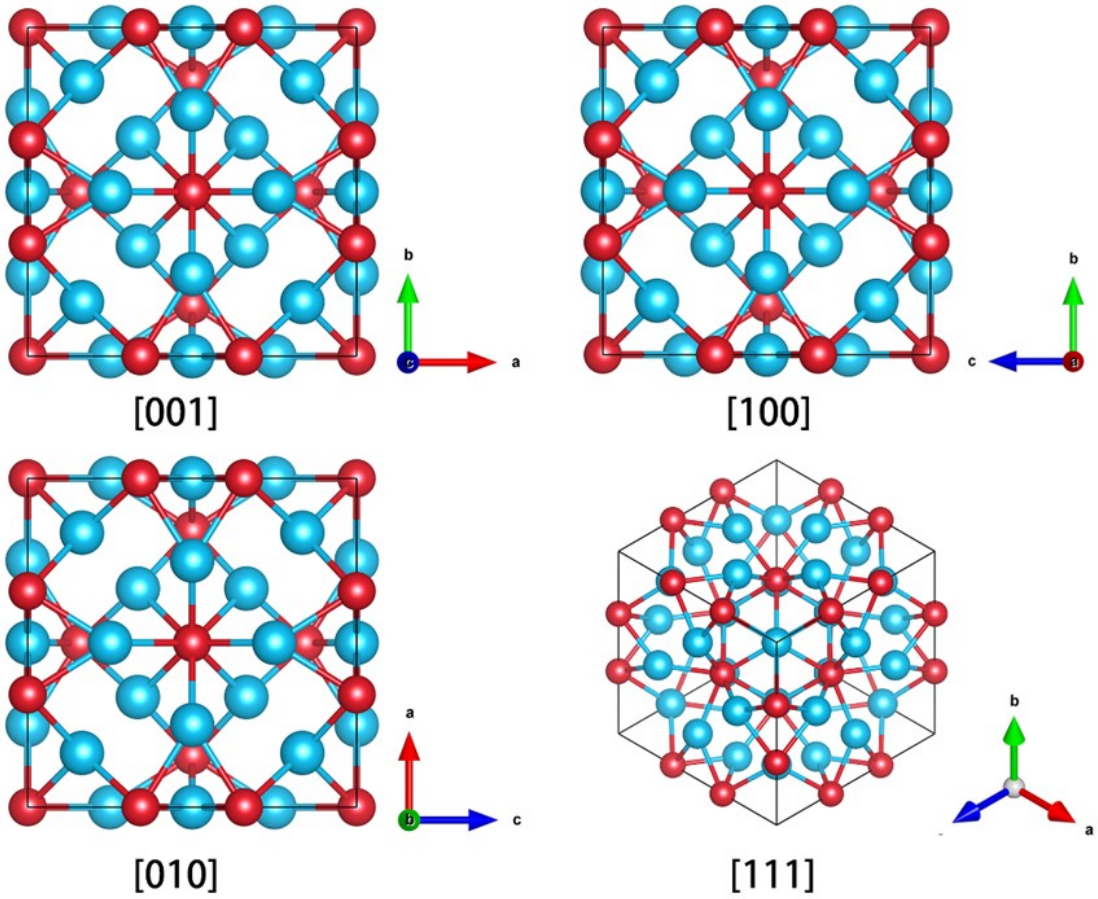

Fig. S2. The crystal structure of Ir_3Sn_7, viewed from [001], [100], [010] and [111] directions, respectively. The red and cyan spheres represent Ir and Sn atoms, respectively.

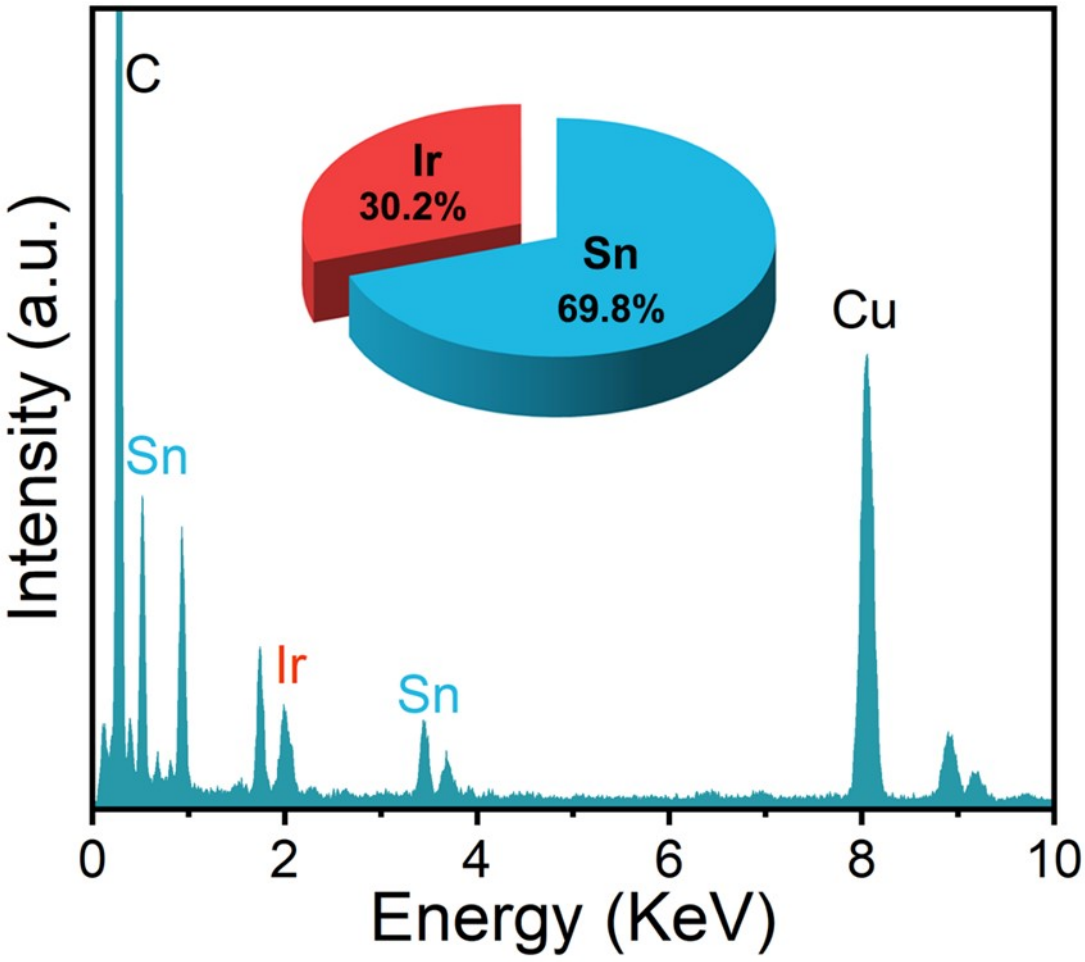

Fig. S3. EDS spectrum of the synthesized Ir_3Sn_7/C.

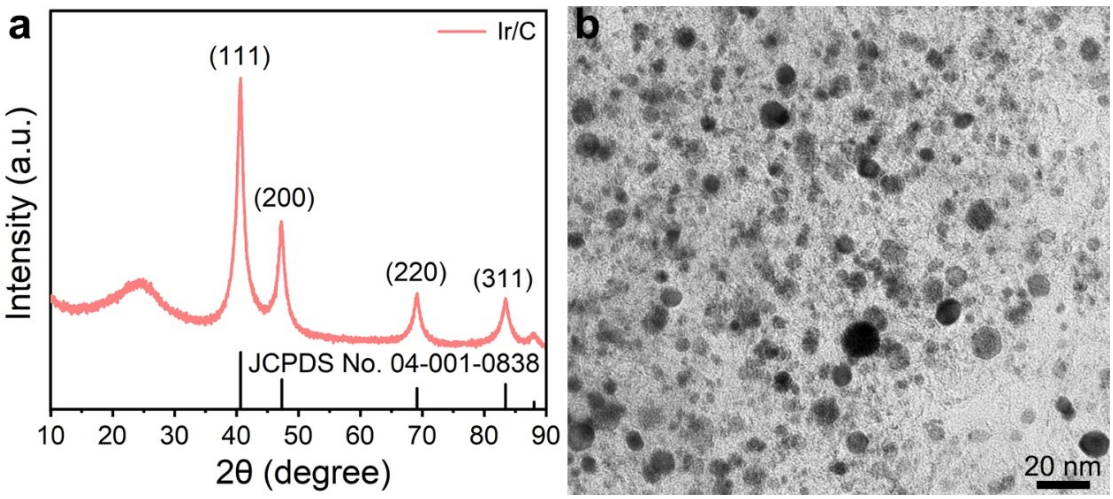

Fig. S4. (a) XRD pattern and (b) Low-magnification TEM image of Ir/C.

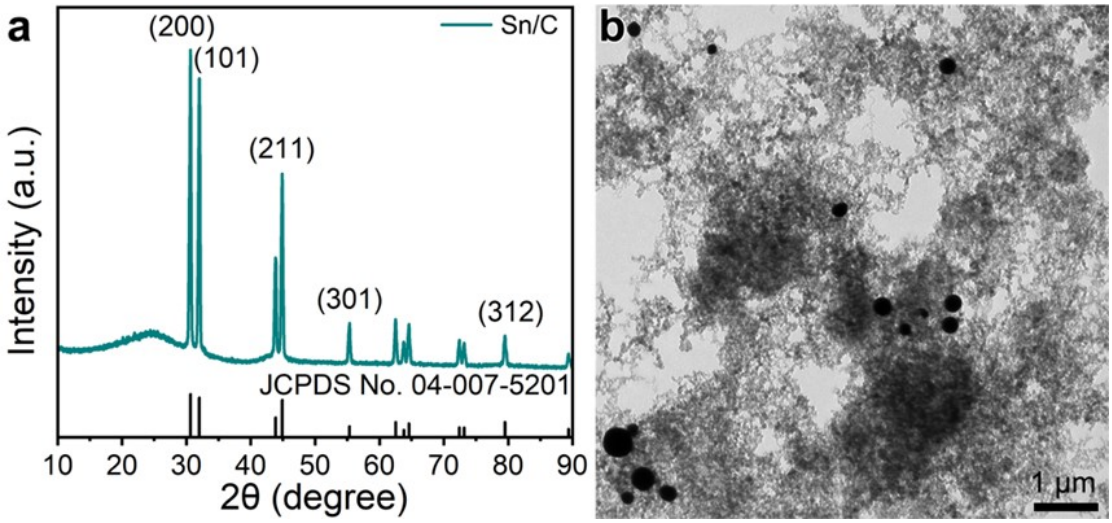

Fig. S5. (a) XRD pattern and (b) Low-magnification TEM image of Sn/C.

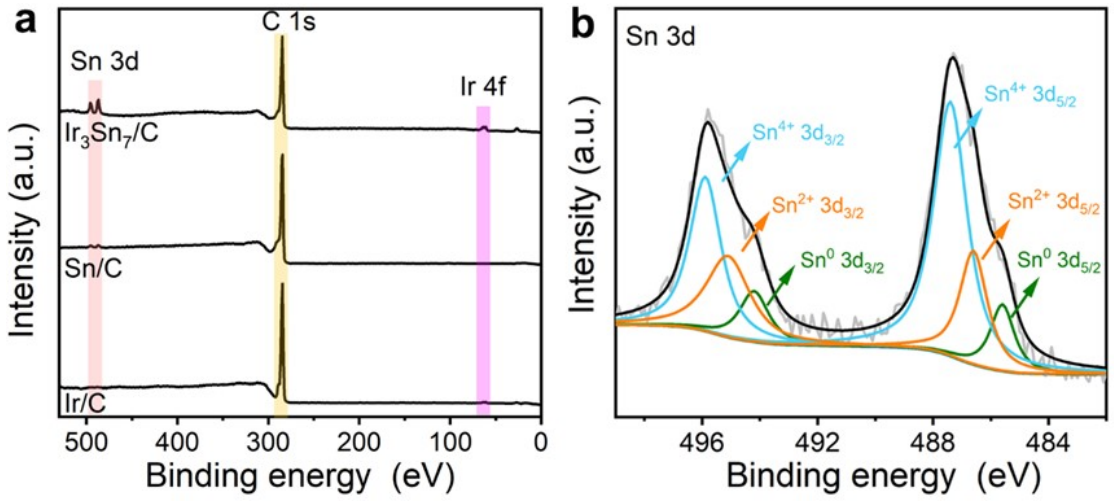

Fig. S6. (a) Full XPS spectra of Ir_3Sn_7/C, Ir/C and Sn/C. (b) High-resolution Sn 3d XPS spectrum of Ir_3Sn_7/C.

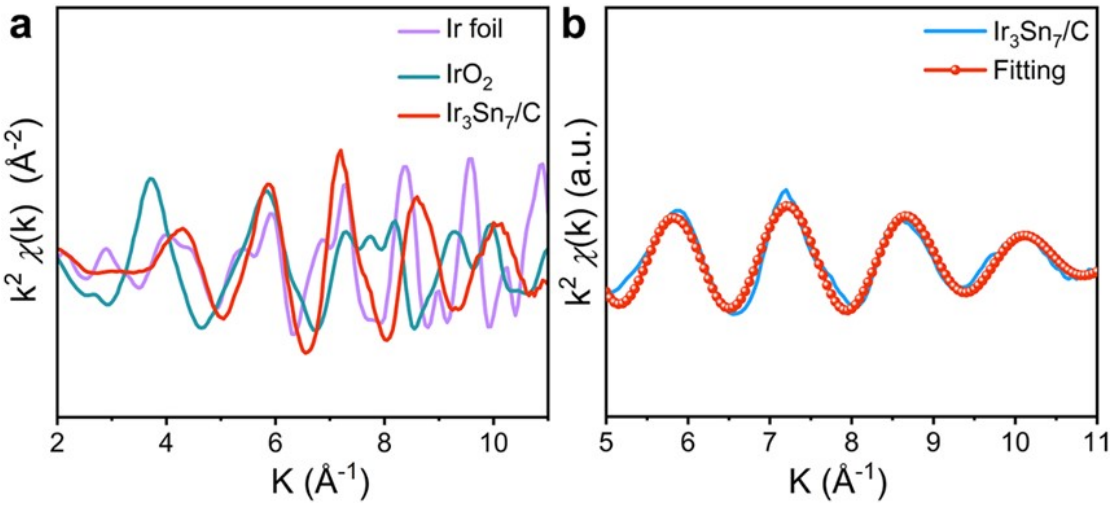

Fig. S7. (a) EXAFS oscillation functions at the Ir L_3-edge of Ir_3Sn_7, Ir foil and IrO_2, respectively. (b) EXAFS oscillation function and fitting curve at the Ir L_3-edge of Ir_3Sn_7/C.

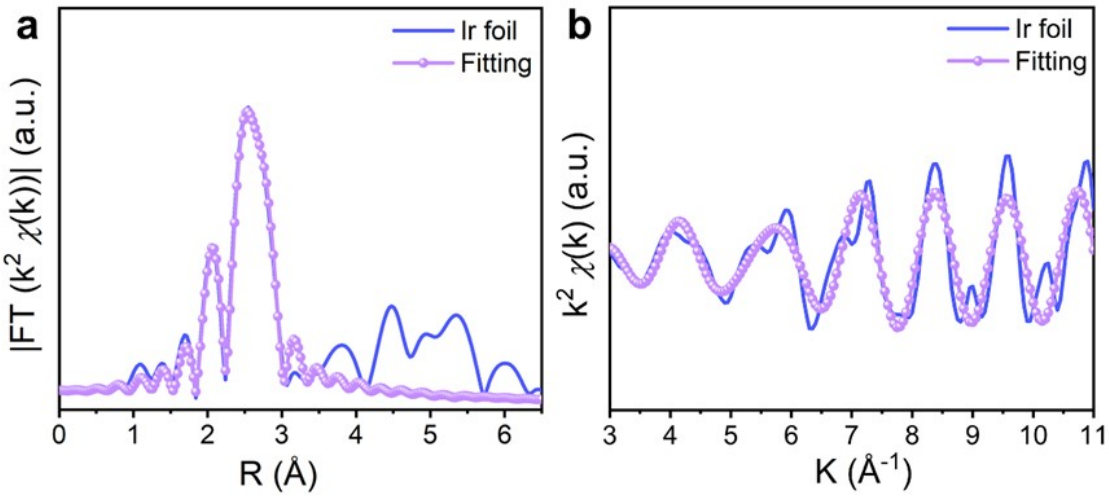

Fig. S8. EXAFS fitting curves of Ir foil at the (a) R space and (b) k space, respectively.

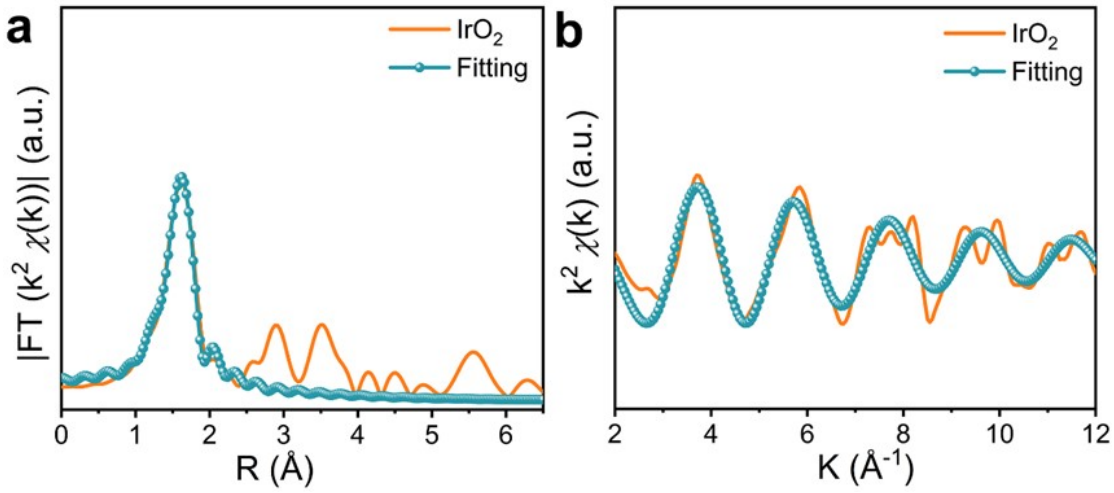

Fig. S9. EXAFS fitting curves of IrO_2 at the (a) R space and (b) k space, respectively.

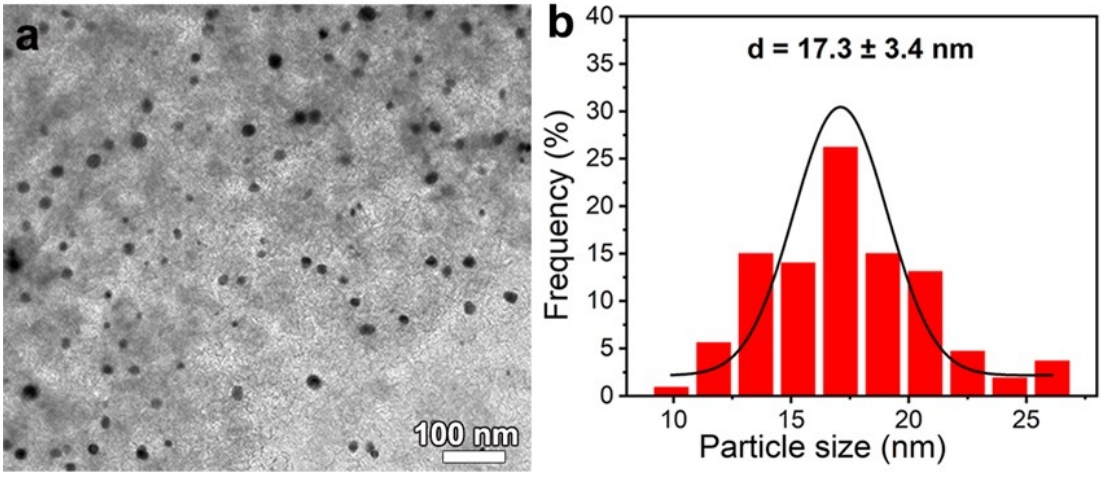

Fig. S10. (a) TEM image of Ru_3Sn_7/C and (b) the particle size distribution of Ru_3Sn_7 IMCs.

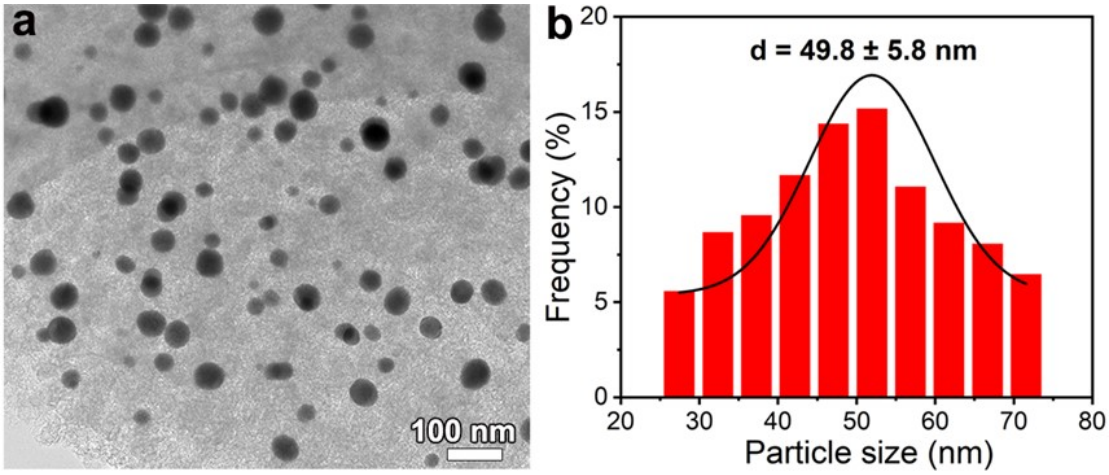

Fig. S11. (a) TEM image of AuSn/C and (b) the particle size distribution of AuSn IMCs.

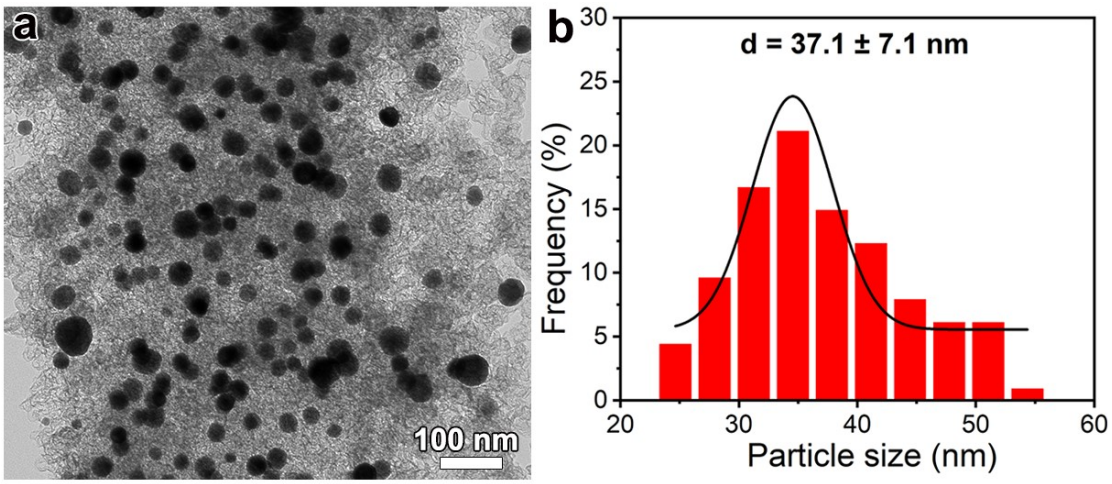

Fig. S12. (a) TEM image of Ag_3Sn/C and (b) the particle size distribution of Ag_3Sn IMCs.

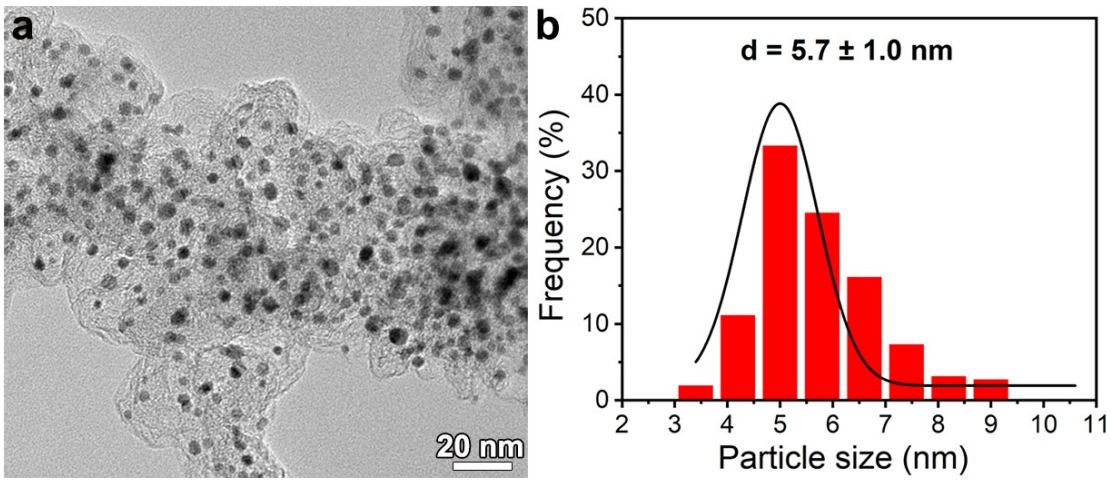

Fig. S13. (a) TEM image of $RuIn_3$/C and (b) the particle size distribution of $RuIn_3$ IMCs.

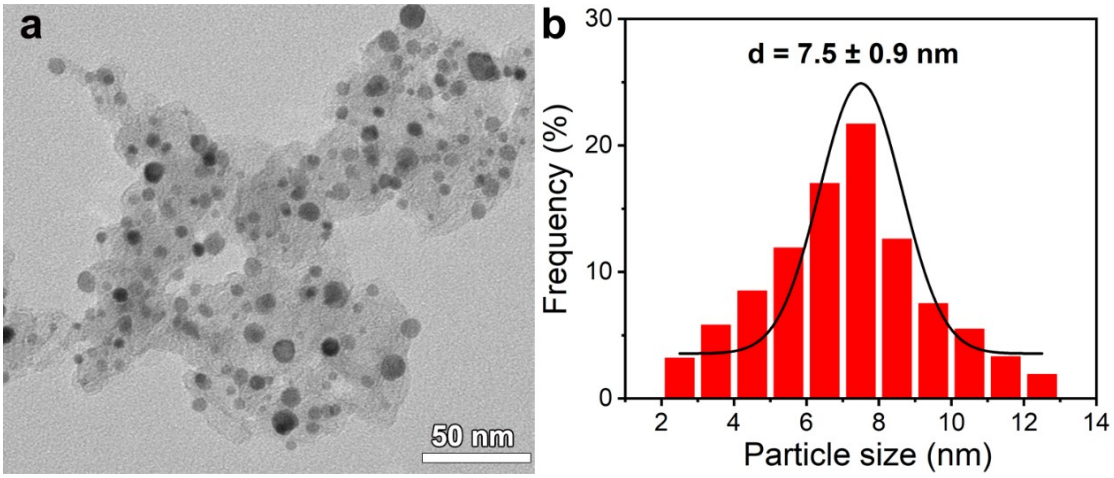

Fig. S14. (a) TEM image of $IrIn_2$/C and (b) the particle size distribution of $IrIn_2$ IMCs.

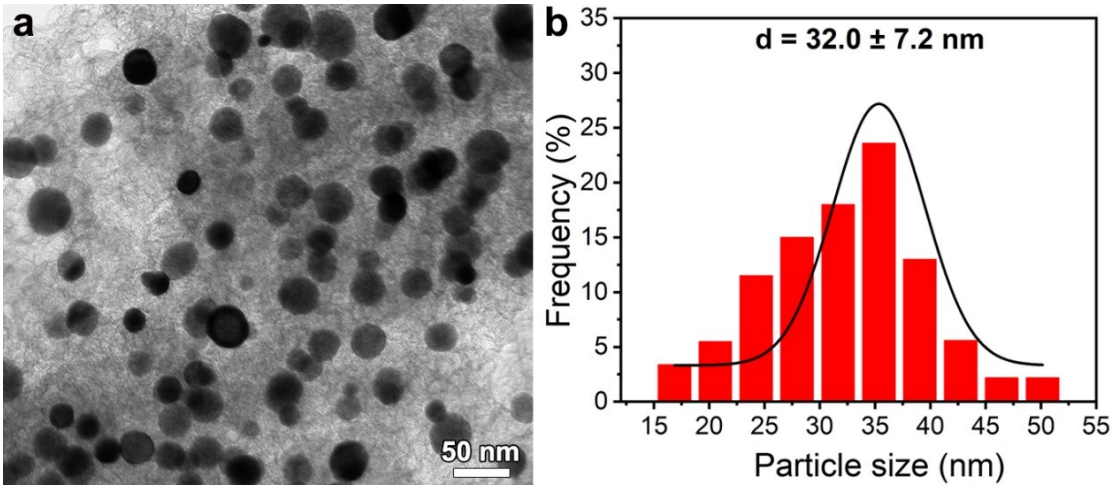

Fig. S15. (a) TEM image of Pd_2In/C and (b) the particle size distribution of Pd_2In IMCs.

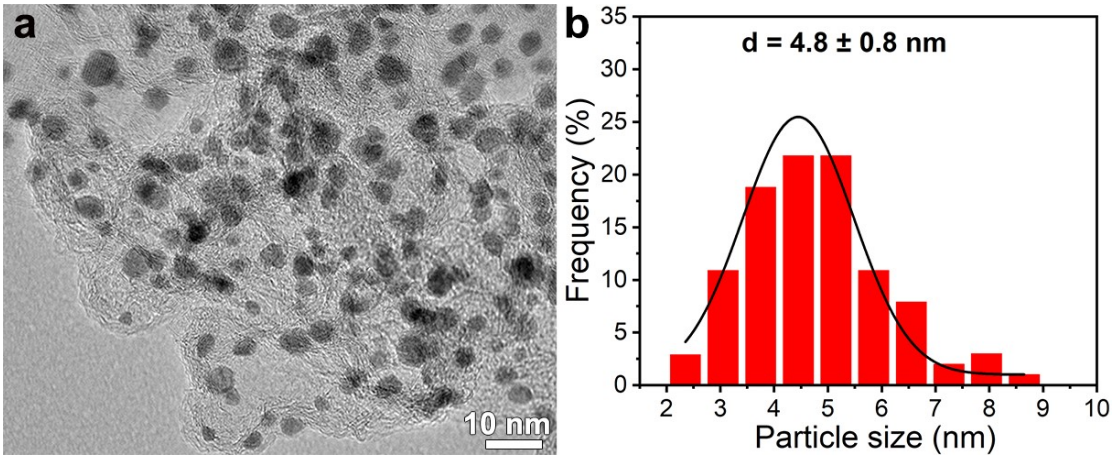

Fig. S16. (a) TEM image of Pt_3In/C and (b) the particle size distribution of Pt_3In IMCs.

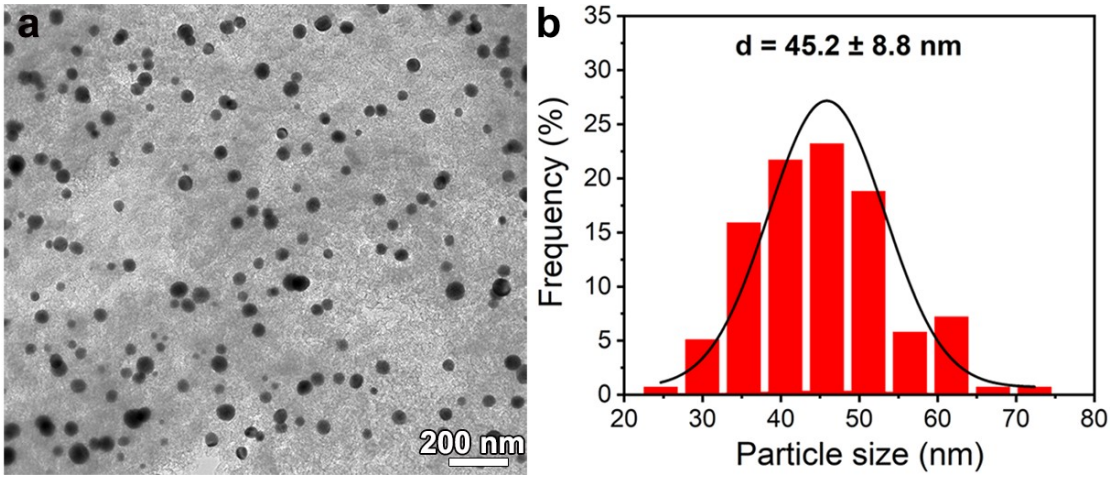

Fig. S17. (a) TEM image of $Au_{10}In_3$/C and (b) the particle size distribution of $Au_{10}In_3$ IMCs.

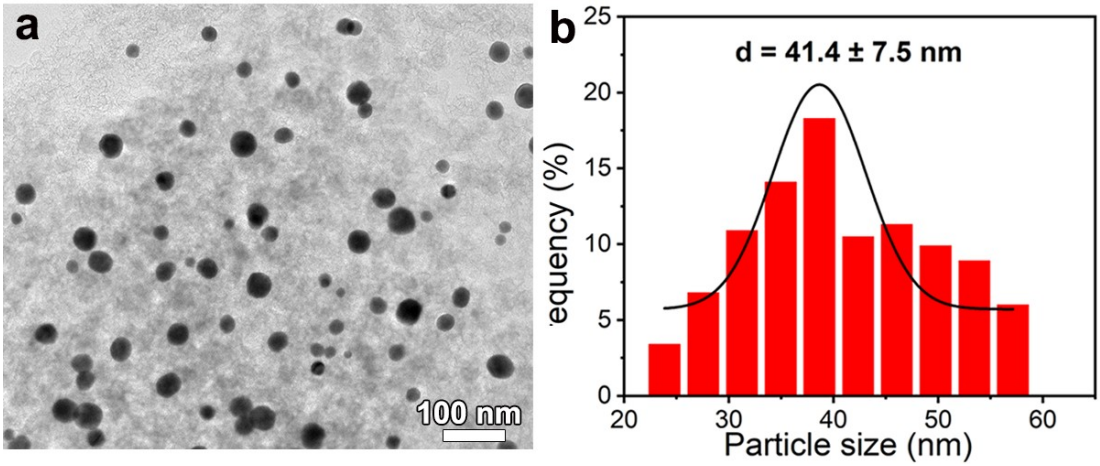

Fig. S18. (a) TEM image of Au_3In/C and (b) the particle size distribution of Au_3In IMCs.

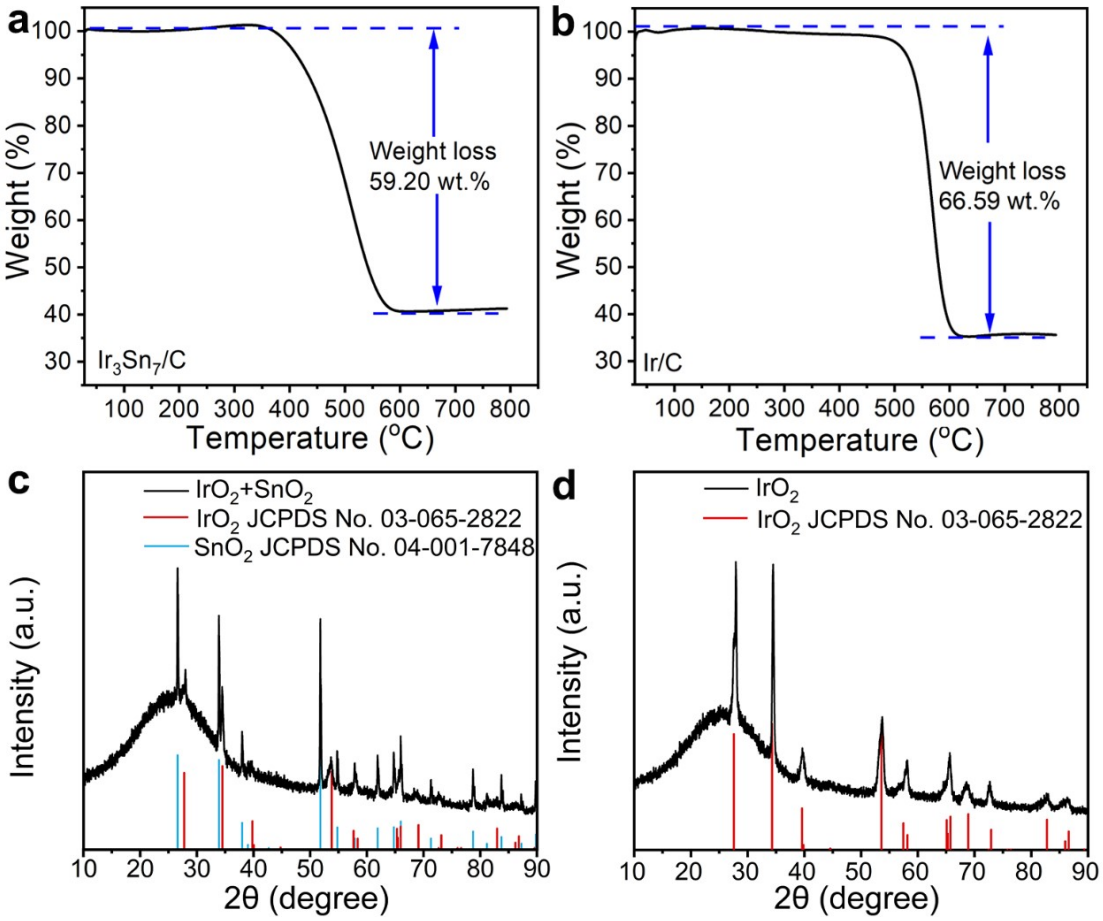

Fig. S19. TGA curves of (a) Ir_3Sn_7/C and (b) Ir/C, respectively. XRD patterns of (c) Ir_3Sn_7/C and (d) Ir/C after TGA measurements. The Ir contents in Ir_3Sn_7/C and Ir/C can be determined by combining TGA and XRD analyses.

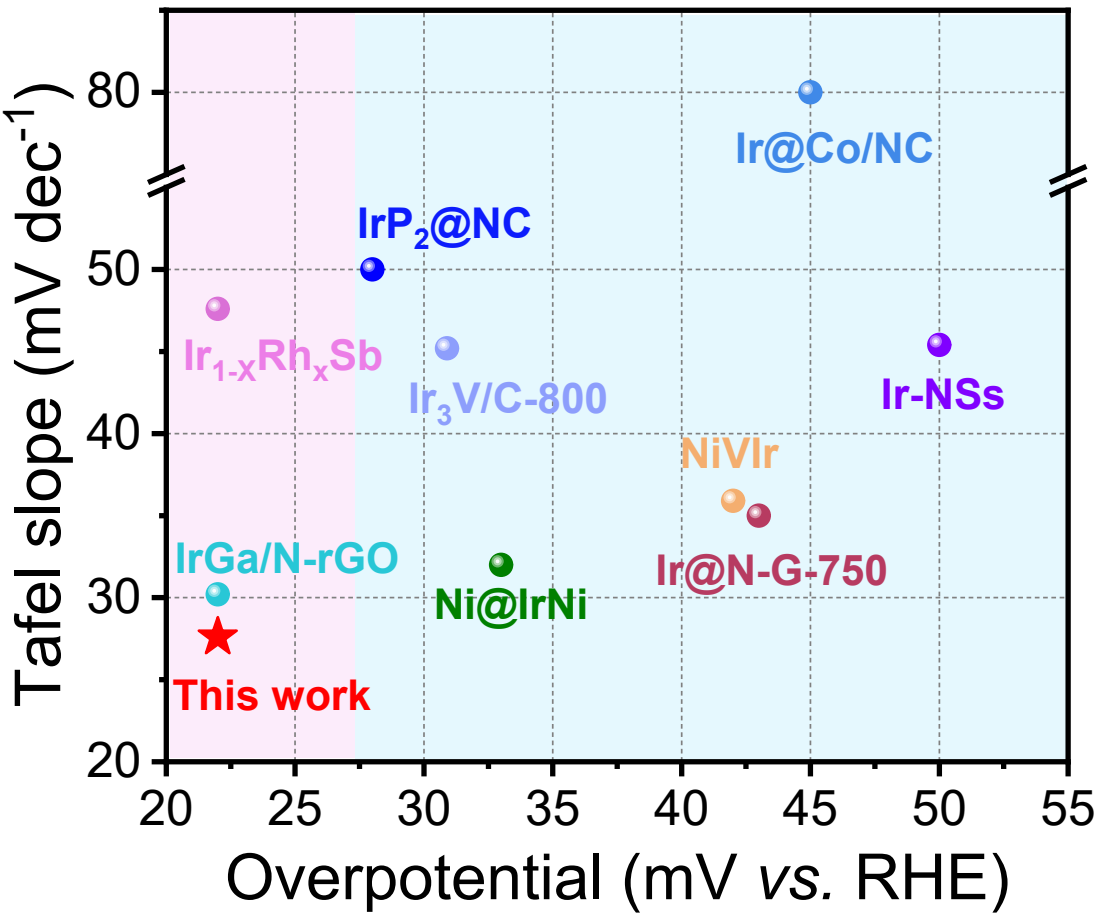

Fig. S20. HER performance comparison using Tafel slope *vs.* overpotential (at 10 mA cm^{-2}) for different Ir-based catalysts.

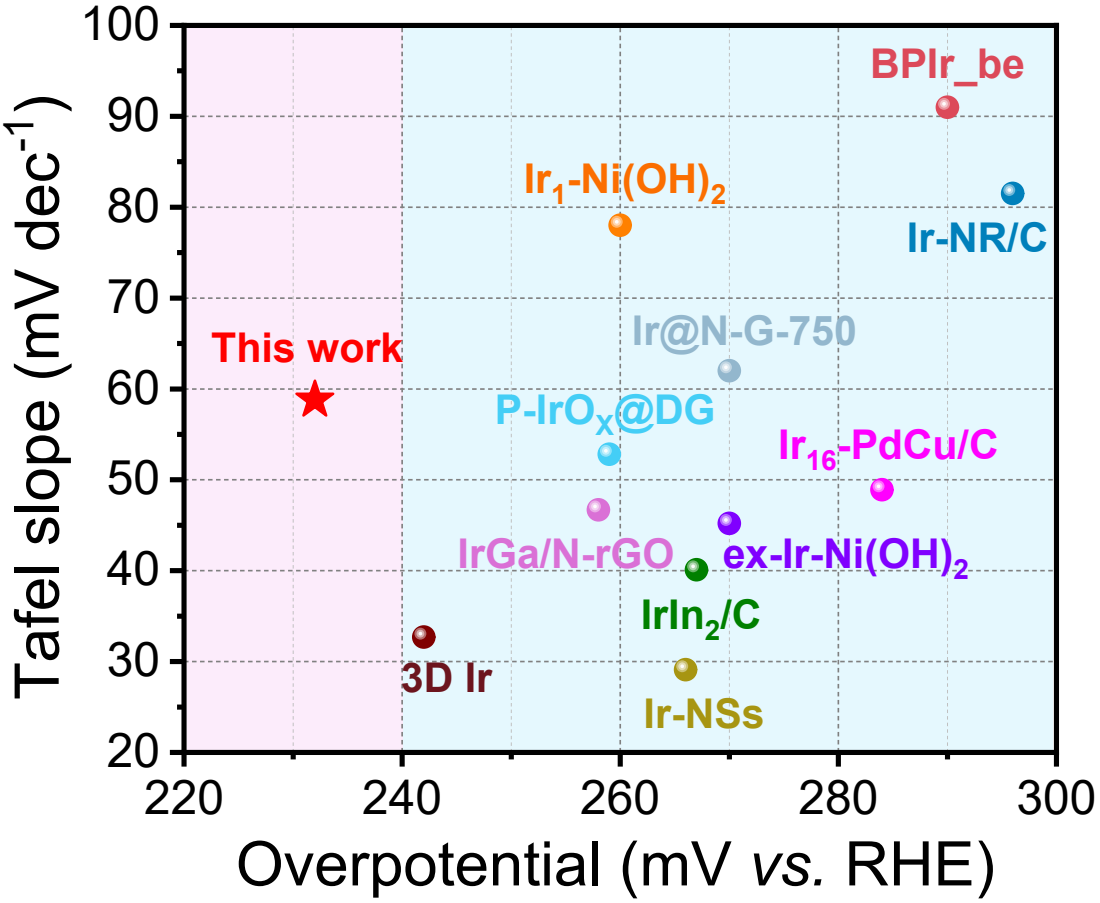

Fig. S21. OER performance comparison using Tafel slope *vs.* overpotential (at 10 mA cm^{-2}) for different Ir-based catalysts.

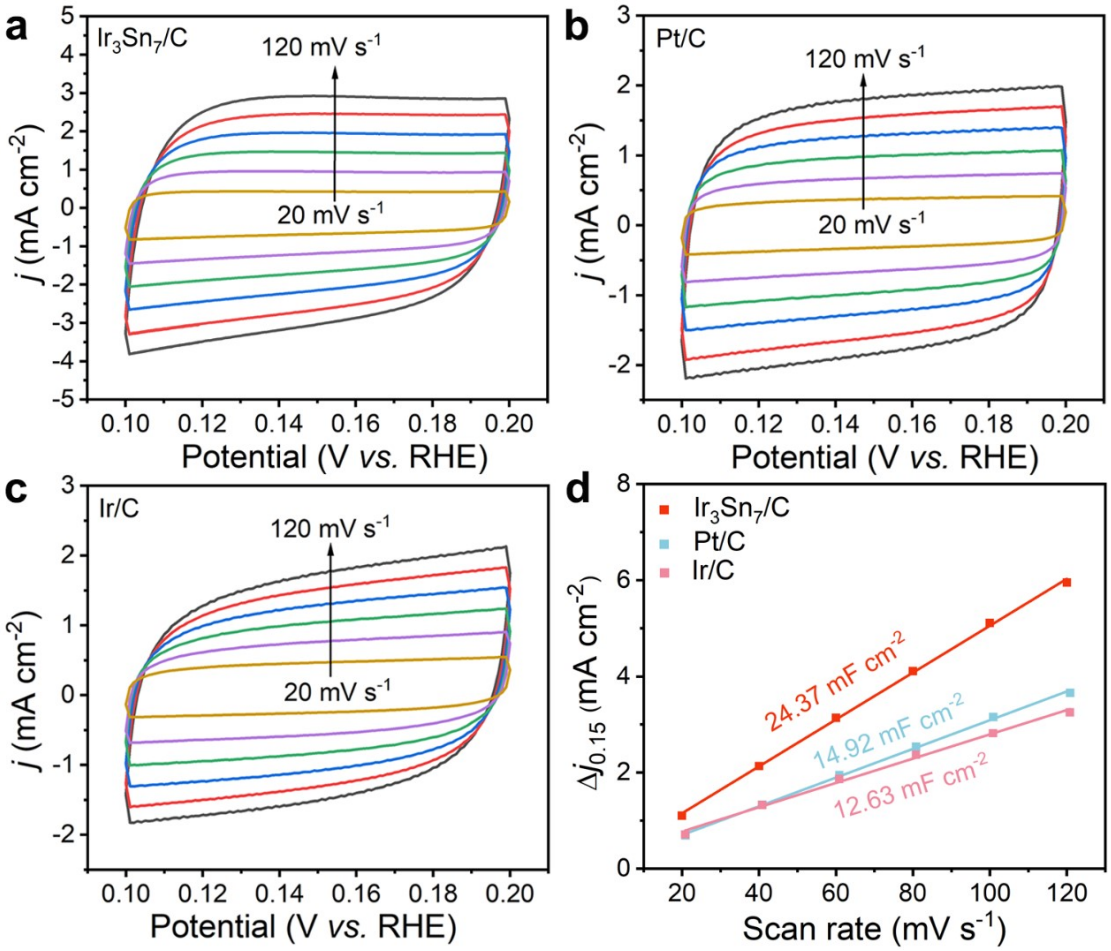

Fig. S22. CV curves of (a) Ir_3Sn_7/C, (b) commercial Pt/C and (c) Ir/C for HER at 0.10 to 0.20 V *vs.* RHE with scan rates from 20 to 120 mV s^{-1}. (d) C_{dl} of Ir_3Sn_7/C, Ir/C and commercial Pt/C, respectively.

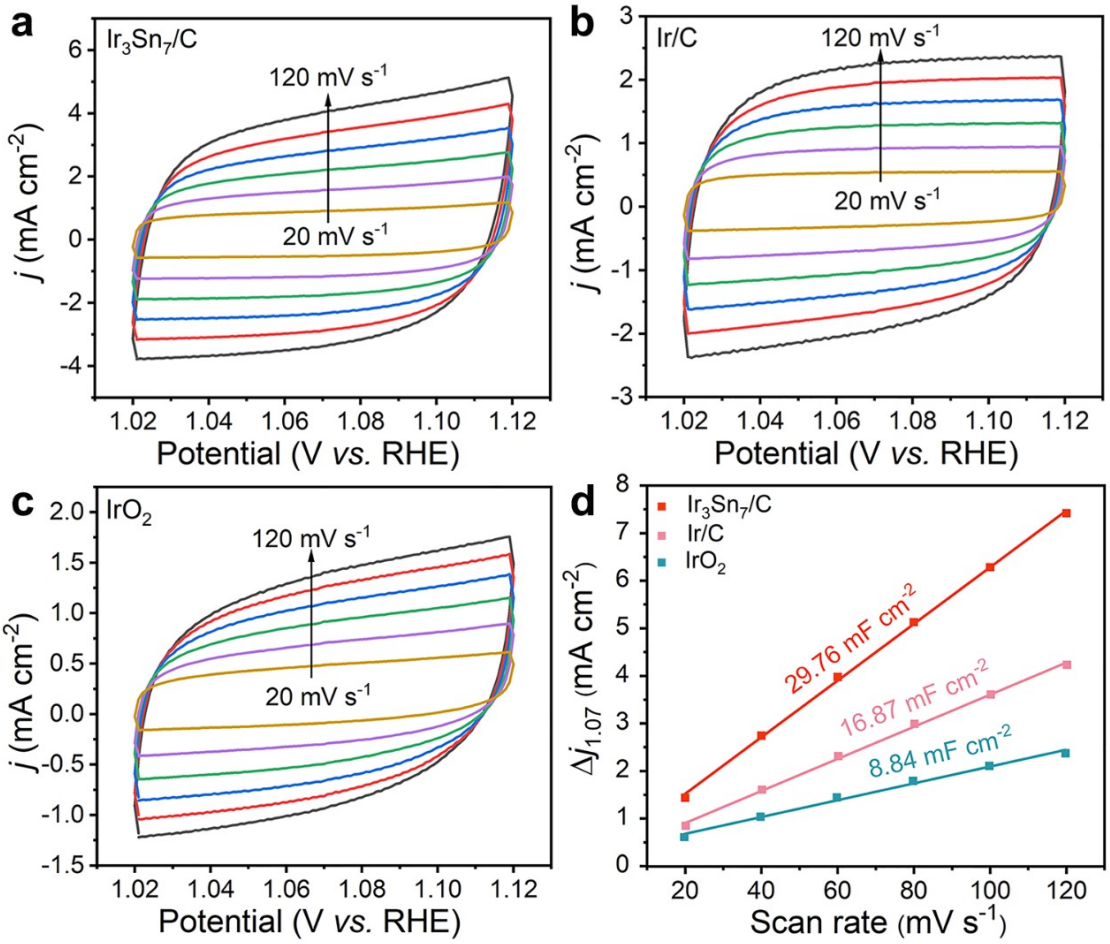

Fig. S23. CV curves of (a) Ir_3Sn_7/C, (b) Ir/C and (c) commercial IrO_2 for OER at 1.02 to 1.12 V *vs.* RHE with scan rates from 20 to 120 mV s^{-1}. (d) C_{dl} of Ir_3Sn_7/C, Ir/C and commercial IrO_2, respectively.

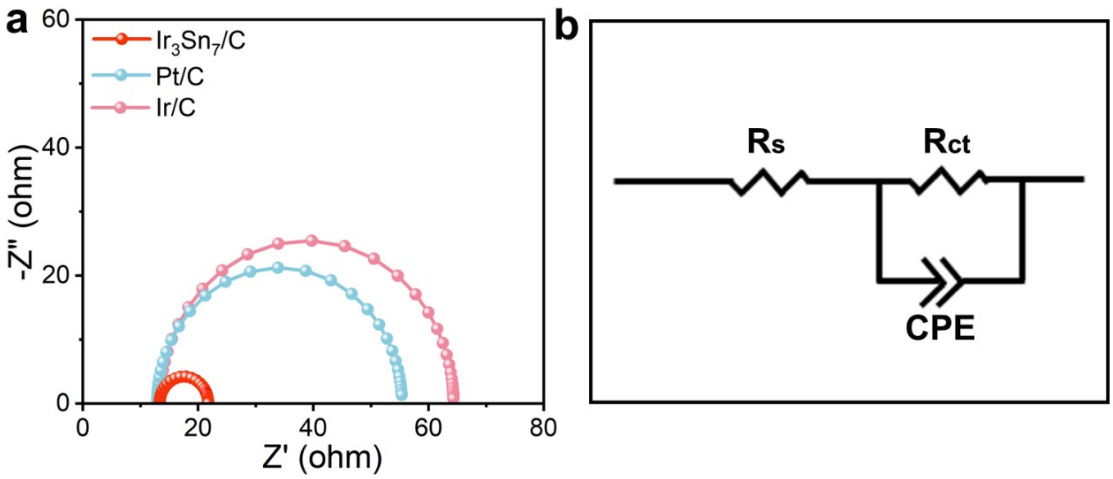

Fig. S24. (a) Nyquist plots of Ir_3Sn_7/C, commercial Pt/C and Ir/C collected in the frequency range of 0.1 Hz-100 kHz at -0.03 V in 1.0 M KOH for HER. (b) The corresponding equivalent electrical circuit. R_s: solution resistance, CPE: constant phase element, R_{ct}: charge transfer resistance.

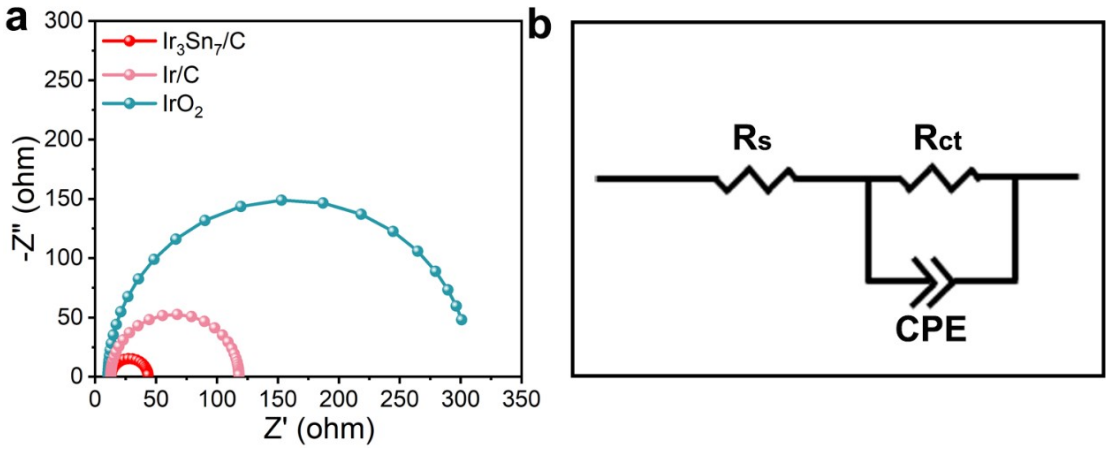

Fig. S25. (a) Nyquist plots of Ir_3Sn_7/C, Ir/C and IrO_2 collected in the frequency range of 0.1 Hz-100 kHz at 1.50 V in 1.0 M KOH for OER. (b) The corresponding equivalent electrical circuit. R_s: solution resistance, CPE: constant phase element, R_{ct}: charge transfer resistance.

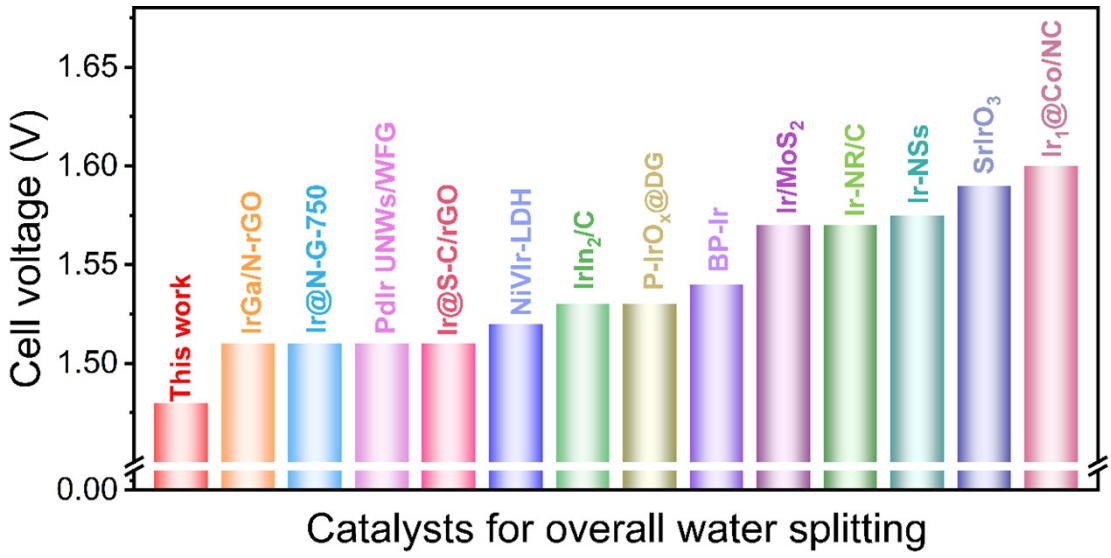

Fig. S26. Comparison of cell voltage of Ir_3Sn_7/C at 10 mA cm^{-2} with recently reported Ir-based catalysts for electrocatalytic overall water splitting.

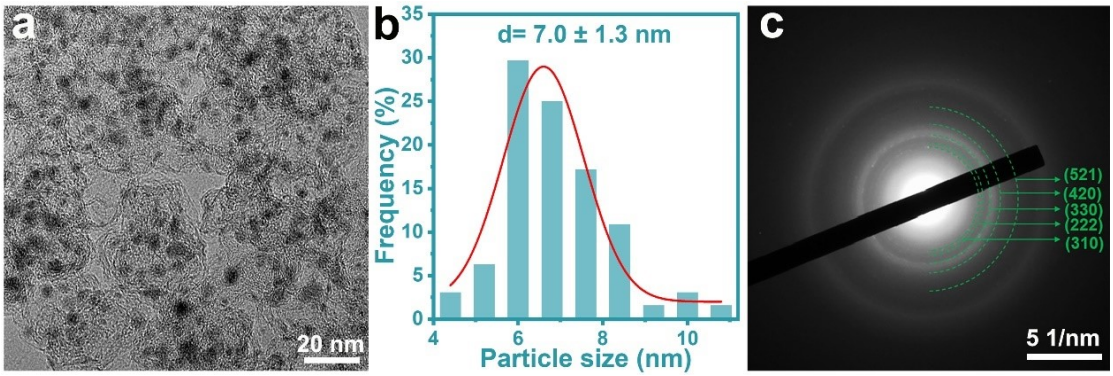

Fig. S27. (a) TEM image, (b) corresponding particle size distribution and (c) SAED pattern of Ir_3Sn_7/C as cathode after the stability test in 1.0 M KOH.

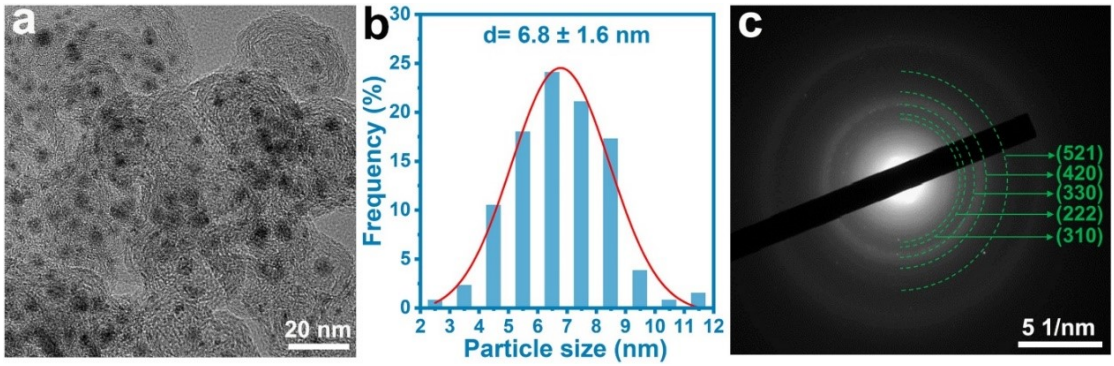

Fig. S28. (a) TEM image, (b) corresponding particle size distribution and (c) SAED pattern of Ir_3Sn_7/C as anode after the stability test in 1.0 M KOH.

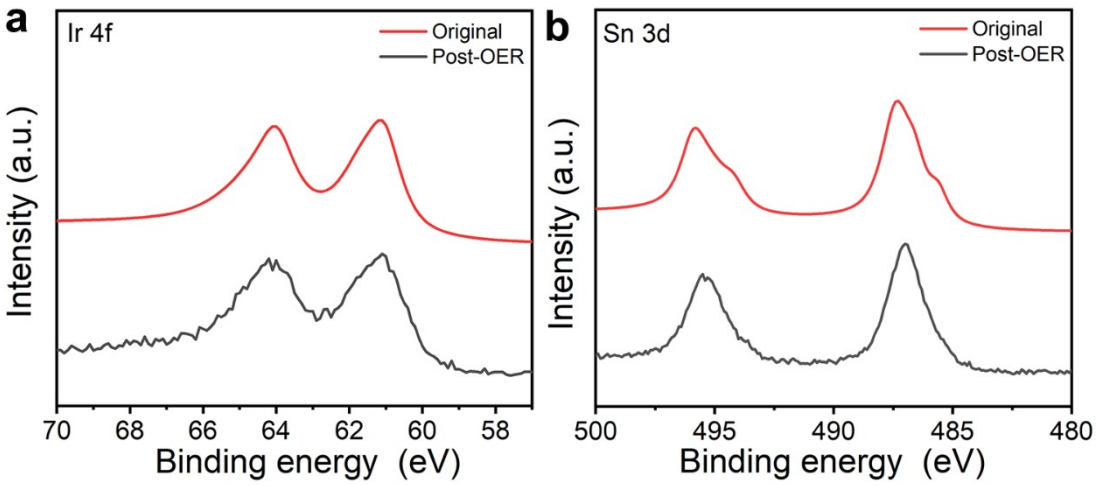

Fig. S29. (a) Ir 4f spectra and (b) Sn 3d spectra of Ir_3Sn_7/C as anode after the stability test in 1.0 M KOH.

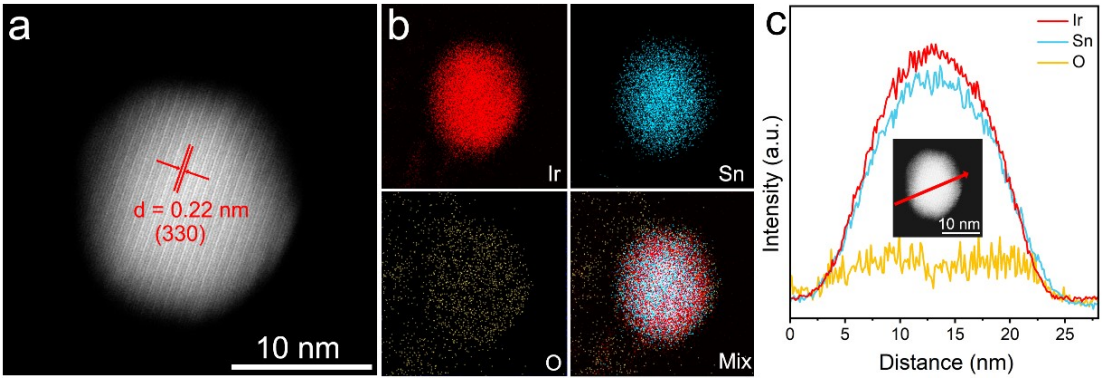

Fig. S30. Structure and morphological characterization of Ir_3Sn_7/C after the OER stability test in 1.0 M KOH. (a) HAADF-STEM image of an individual Ir_3Sn_7 IMC nanoparticle. (b) The corresponding EDS elemental mapping images. (c) The EDS line scan profile of Ir_3Sn_7 IMC.

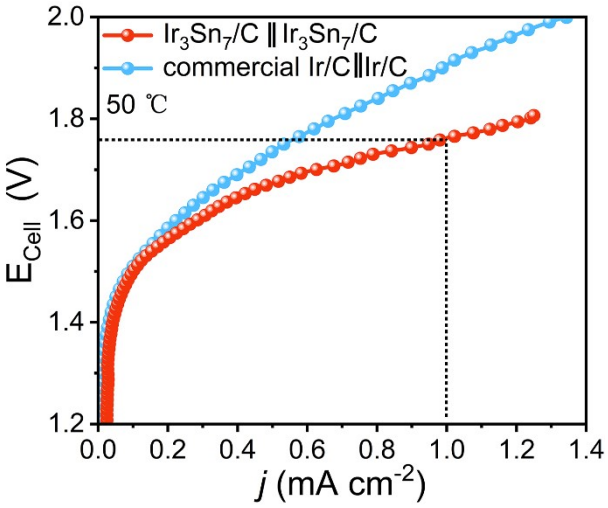

Fig. S31. I-V curves of the AEM water electrolyzer with different catalysts at 50 °C.

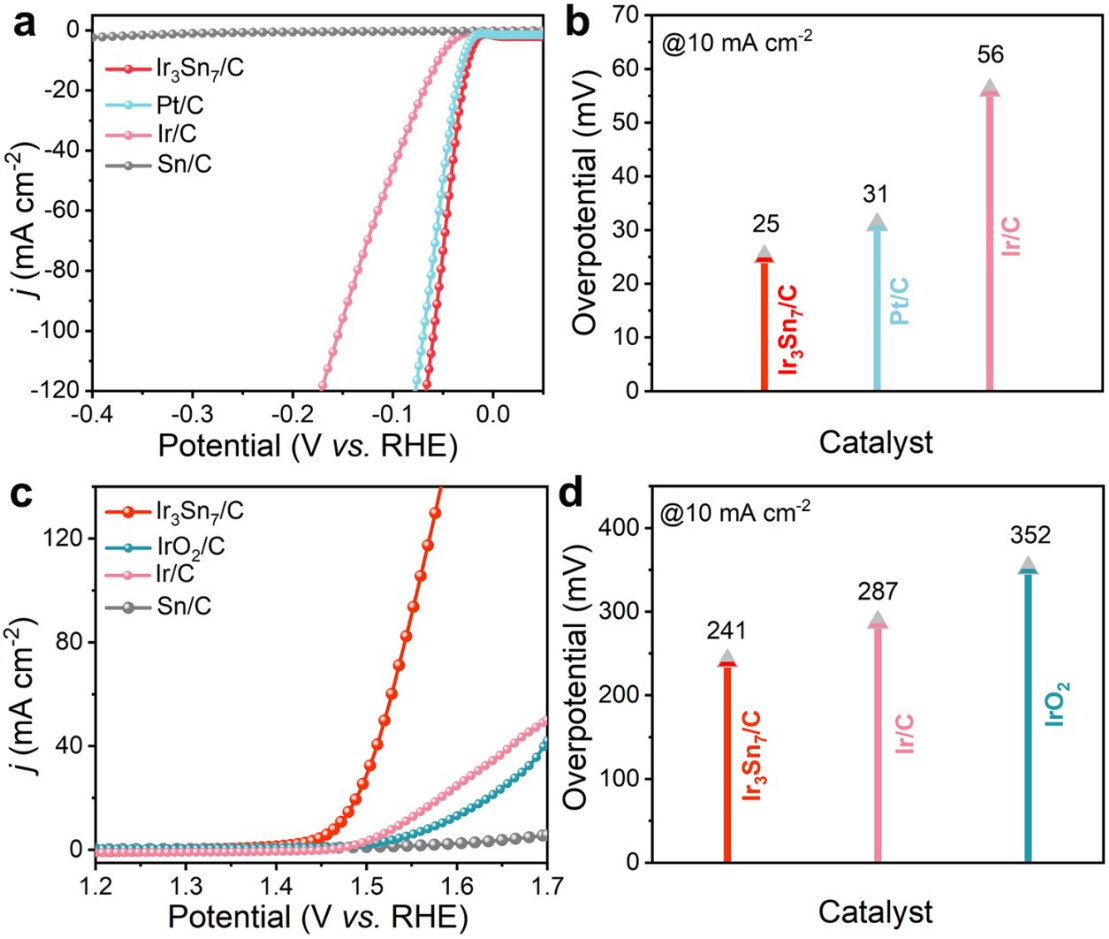

Fig. S32. (a) HER polarization curves with *iR* compensation of Ir_3Sn_7/C, Ir/C, Sn/C and commercial Pt/C in 0.5 M H_2SO_4, respectively. (b) Comparison of overpotentials at the current density of 10 mA cm^{-2}. (c) OER polarization curves with *iR* compensation of Ir_3Sn_7/C, Ir/C, Sn/C and IrO_2 in 0.5 M H_2SO_4, respectively. (d) Comparison of overpotentials at the current density of 10 mA cm^{-2}.

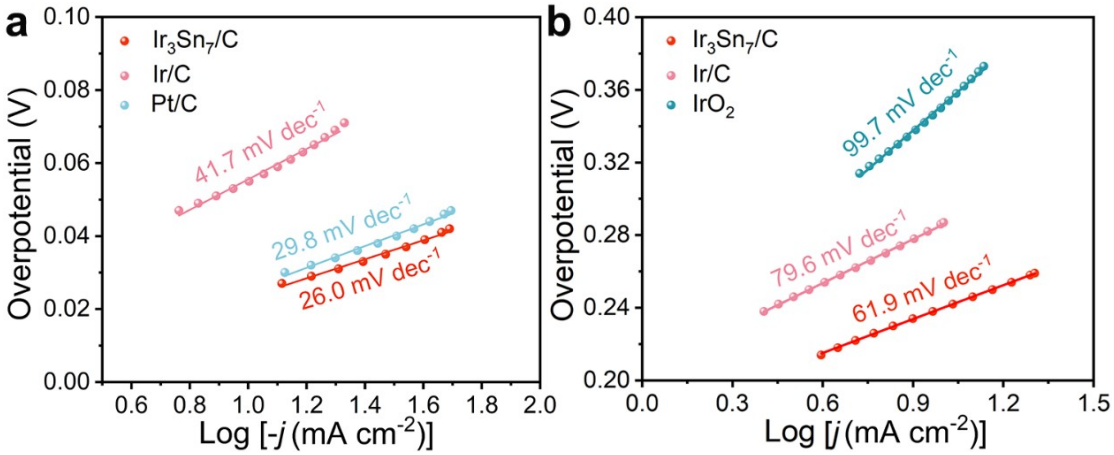

Fig. S33. (a) Tafel slopes values of the Ir_3Sn_7/C, Ir/C and commercial Pt/C in 0.5 M H_2SO_4 for HER. (b) Tafel slopes values of the Ir_3Sn_7/C, Ir/C and commercial IrO_2 in 0.5 M H_2SO_4 for OER.

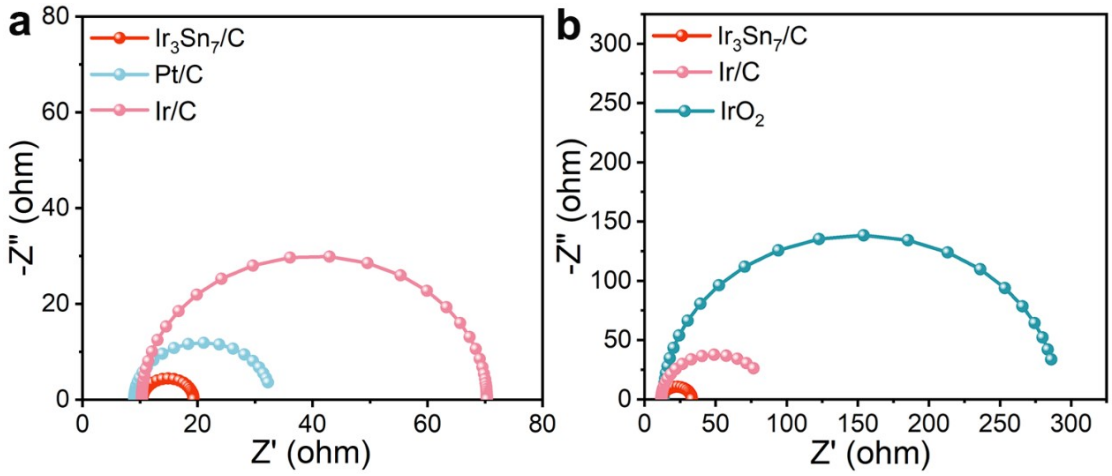

Fig. S34. (a) Nyquist plots for Ir_3Sn_7/C, Ir/C and Pt/C in 0.5 M H_2SO_4 for HER. (b) Nyquist plots for Ir_3Sn_7/C, Ir/C and IrO_2 in 0.5 M H_2SO_4 for OER.

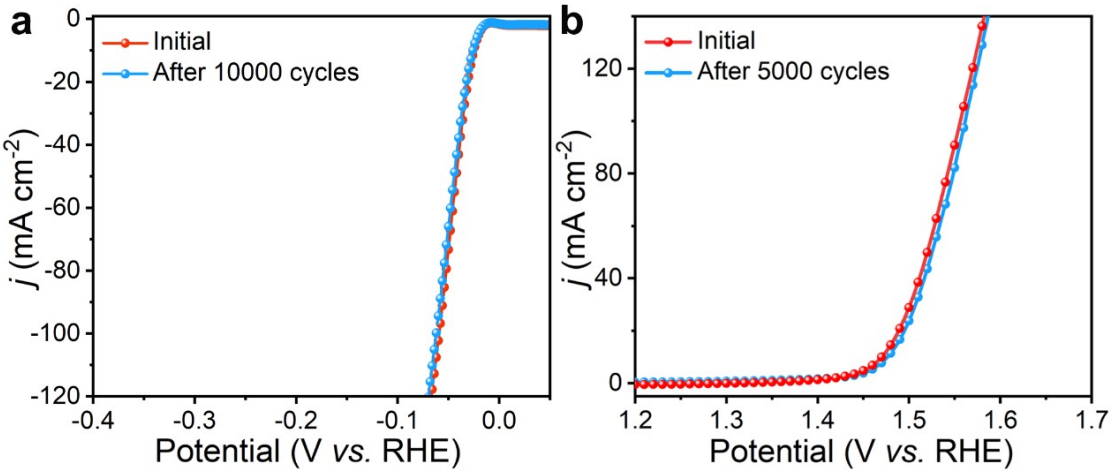

Fig. S35. (a) LSV polarization curves of Ir_3Sn_7/C before and after 10,000 cycles for HER in 0.5 M H_2SO_4. (b) LSV polarization curves of Ir_3Sn_7/C before and after 5,000 cycles for OER in 0.5 M H_2SO_4.

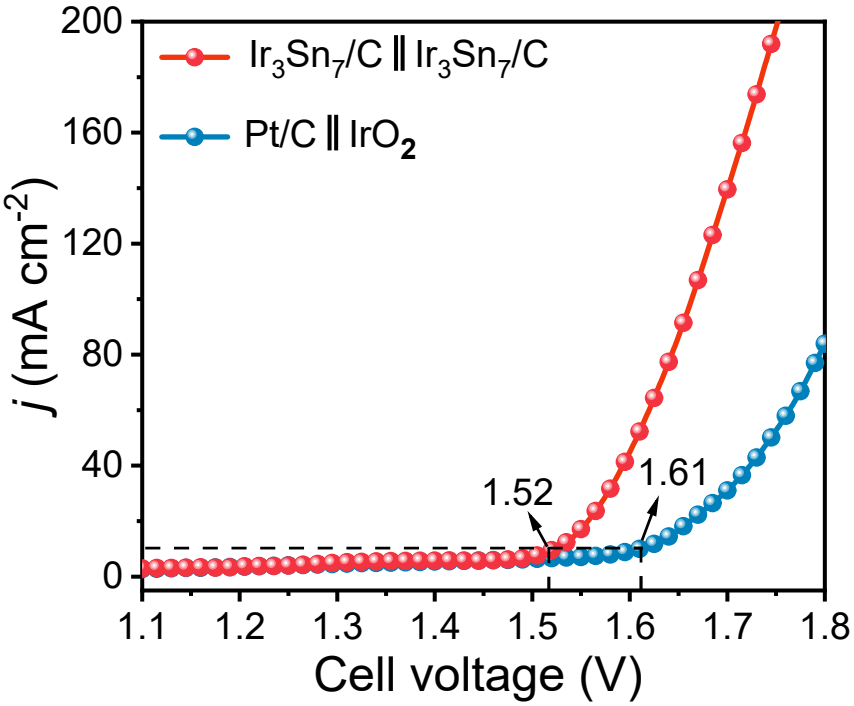

Fig. S36. The *iR*-corrected LSV polarization curves of Ir_3Sn_7/C||Ir_3Sn_7/C and commercial Pt/C||IrO_2 for overall water splitting in 0.5 M H_2SO_4.

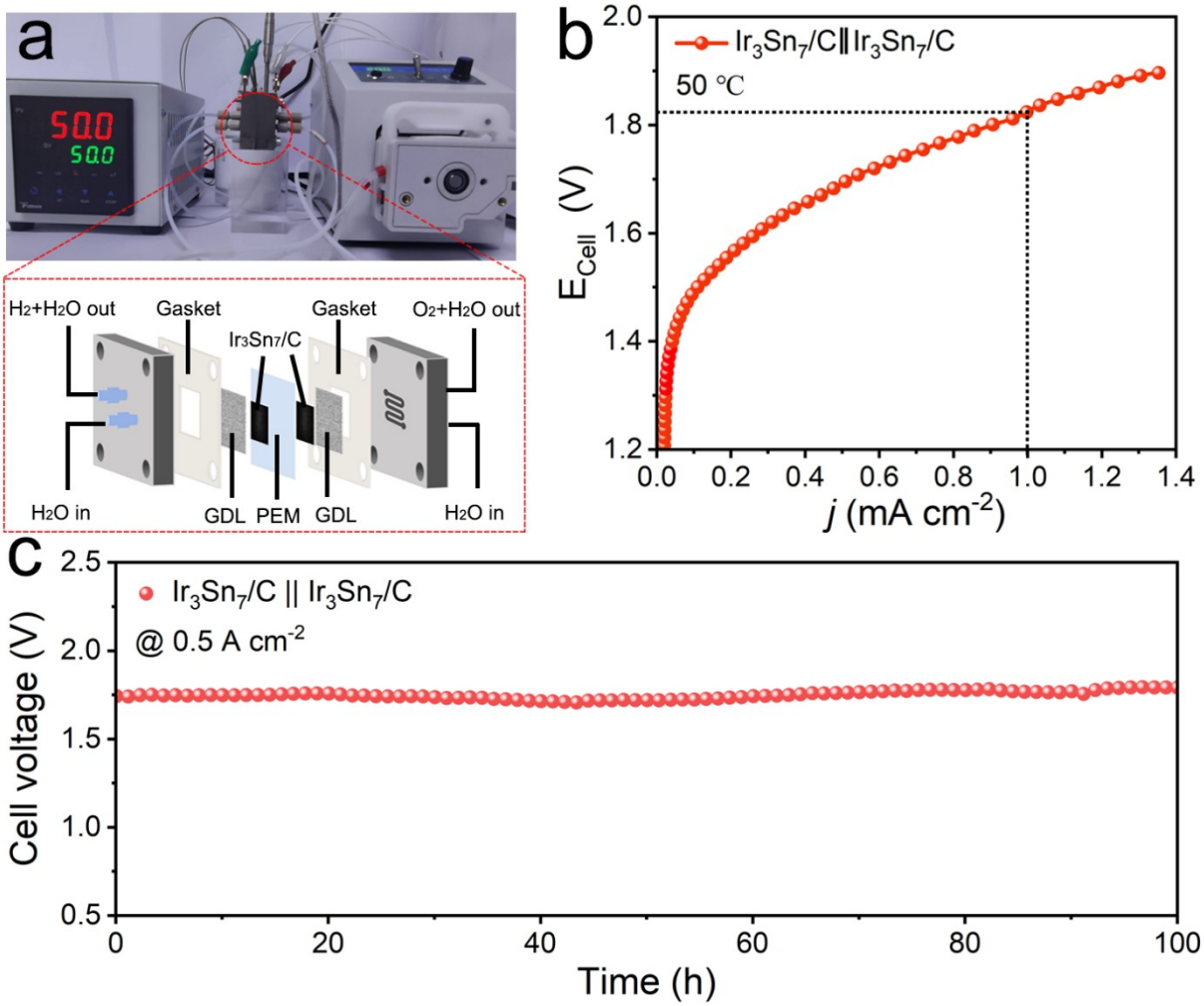

Fig. S37. (a) Photograph of the PEM water electrolysis device (the inset shows a schematic diagram of the PEM water electrolyzer). (b) Polarization curves of the PEM water electrolyzer using the prepared Ir_3Sn_7/C as both anode and cathode with the PEM water electrolyzer at 50 °C. (c) Chronopotentiometry tests of Ir_3Sn_7/C || Ir_3Sn_7/C at 0.5 A cm^{-2} in 0.5 M H_2SO_4.

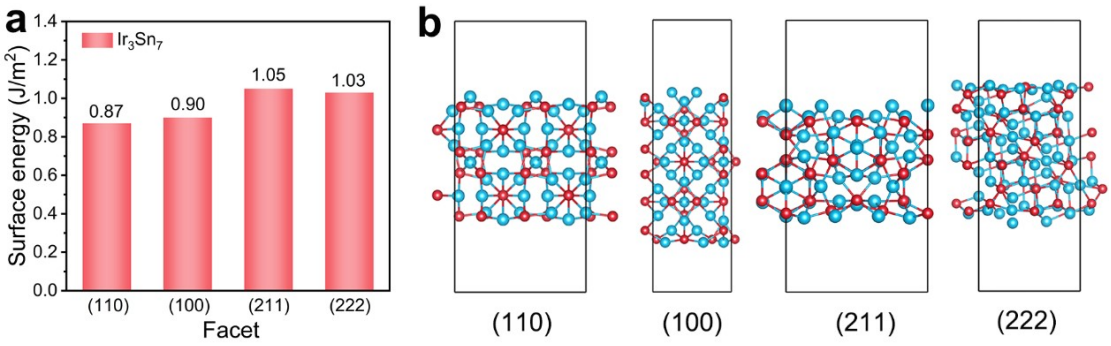

Fig. S38. (a) Surface energies of Ir_3Sn_7 (110), (100), (211) and (222) facets and (b) the corresponding crystal models.

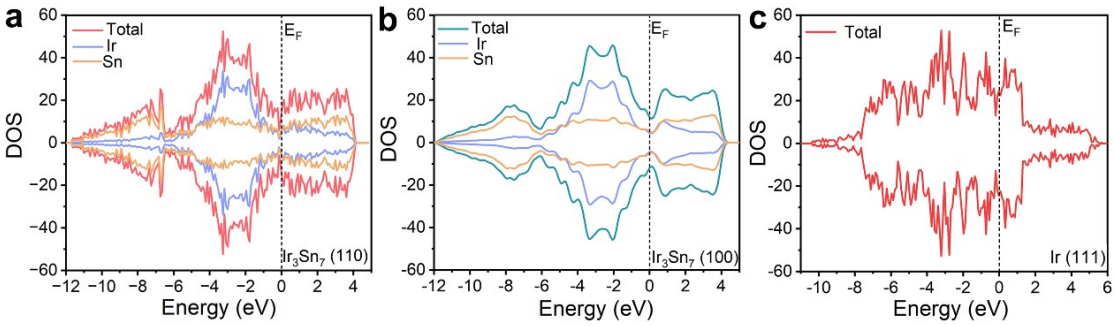

Fig. S39. Calculated DOSs of (a) Ir_3Sn_7 (110), (b) Ir_3Sn_7 (100) and (c) Ir (111).

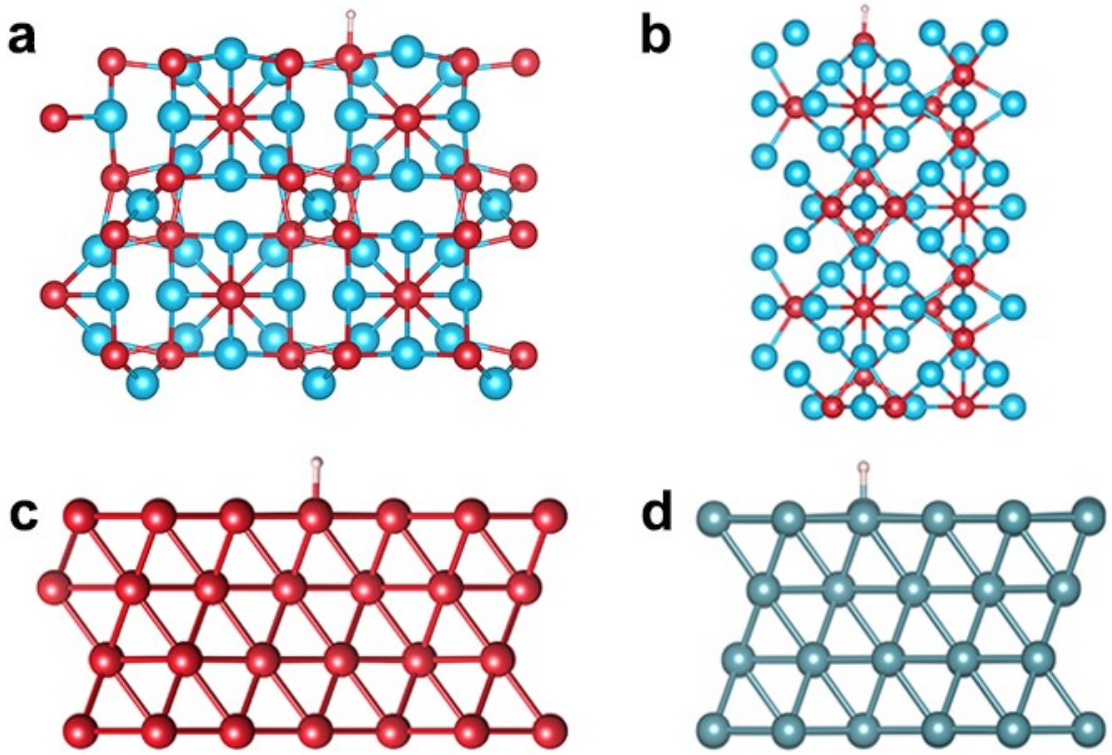

Fig. S40. Optimized structural models of *H on the surface of (a) Ir_3Sn_7 (110), (b) Ir_3Sn_7 (100), (c) Ir (111) and (d) Pt (111).

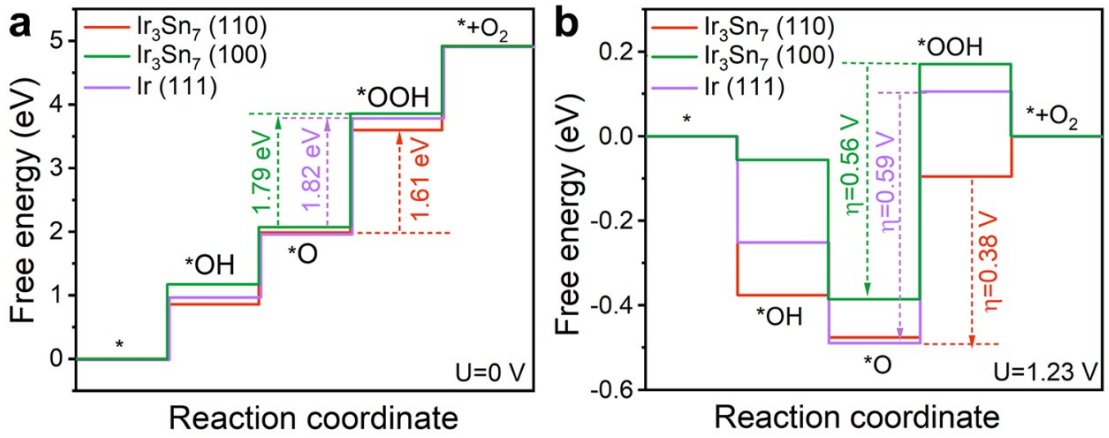

Fig. S41. The free energy diagrams of OER process on Ir_3Sn_7 (110), Ir_3Sn_7 (100) and Ir (111) under the applied overpotential of (a) 0 and (b) 1.23 V respectively.

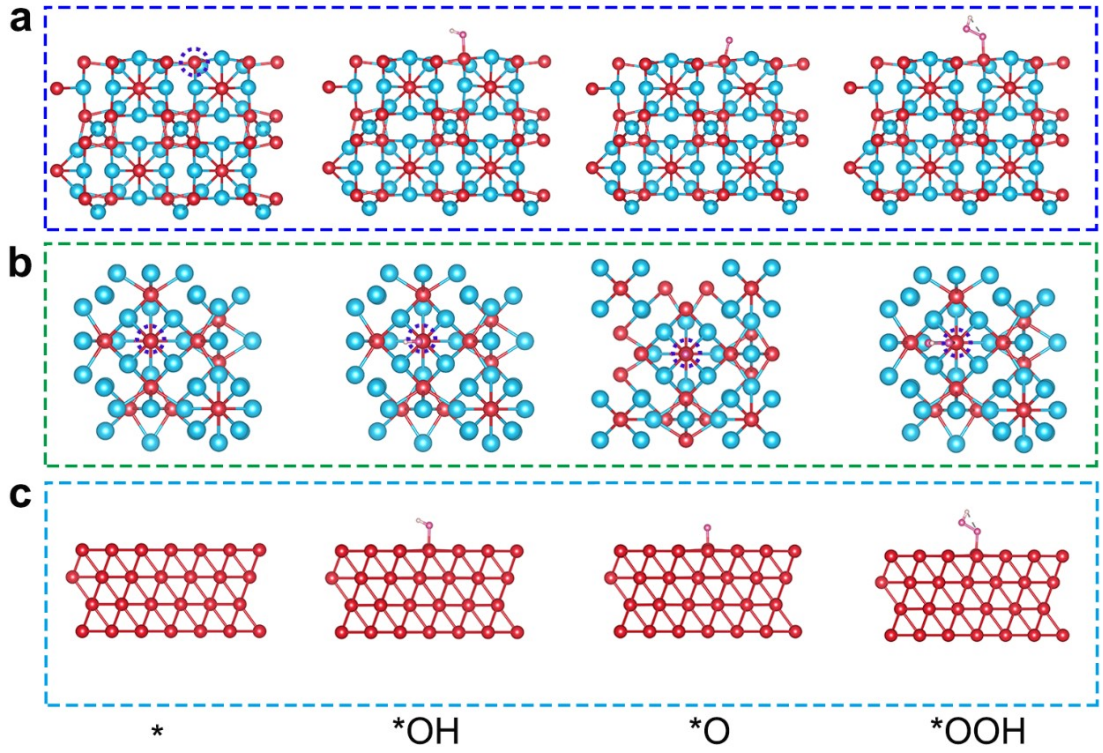

Fig. S42. Structural models of intermediates on (a) Ir_3Sn_7 (110), (b) Ir_3Sn_7 (100) and (c) Ir (111) in the OER process.

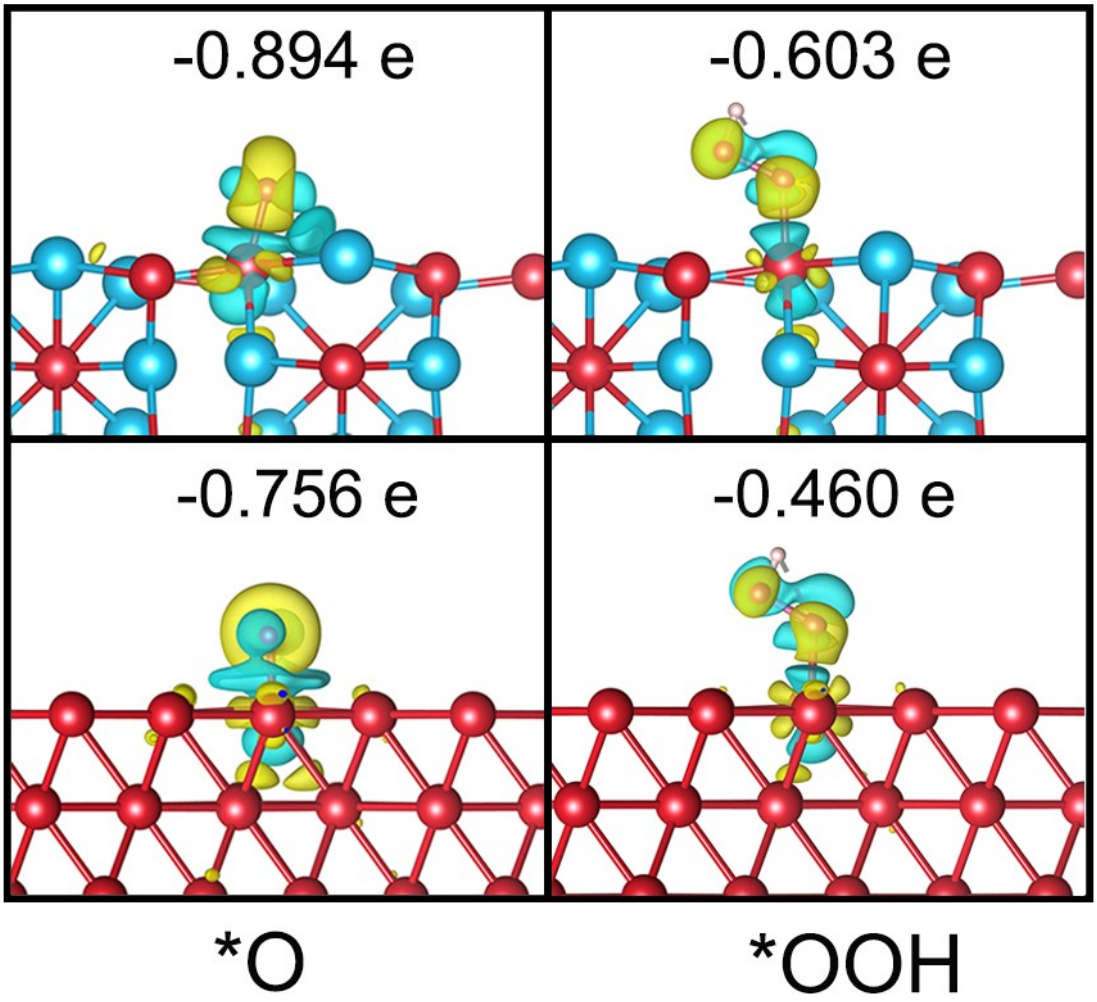

Fig. S43. 3D charge density difference maps and Bader charge analyses of *O and *OOH intermediates on Ir_3Sn_7 (110) and Ir (111). The isosurface value is set to 0.004 e $Å^{-3}$. Yellow and cyan regions represent the electron accumulation and deletion, respectively.

Supplementary Tables

Table S1. The lattice parameters of the Ir_3Sn_7 IMCs determined by the Rietveld refinement analysis. And the theoretical values from Inorganic Crystal Structure Database (ICSD) are also provided.

Simulated values		**Theoretical values**
Space group	$Im\bar{3}m$	$Im\bar{3}m$
a (Å)	9.353	9.352
b (Å)	9.353	9.352
c (Å)	9.353	9.352
α (°)	90°	90°
β (°)	90°	90°
γ (°)	90°	90°

Table S2. EXAFS fitting parameters at the Ir L_3-edge for three samples (S_0^2=0.75).

Sample	Path	CN	R (Å)	σ^2 (Å^2)	ΔE_0 (eV)	R factor (%)
Ir foil	Ir-Ir	12*	2.71±0.01	0.0032	9.2	0.0076
IrO_2	Ir-O	6.0±0.2	1.98±0.01	0.0020	11.6	0.0060
Ir_3Sn_7	Ir-Sn	8.0	2.54±0.01	0.0121	-14.2	0.0118

[a]*CN*, coordination number; [b]*R*, distance between absorber and backscatter atoms; [c]σ^2, Debye-Waller factor to account for both thermal and structural disorders; [d]ΔE_0, inner potential correction; *R* factor indicates the goodness of the fit. S_0^2 was fixed to 0.75, according to the experimental EXAFS fit of Ir foil by fixing CN as the known crystallographic value.

Table S3. Type and dosage of noble metals precursors and p-block element precursors used for the synthesis of noble metal-p-block-element IMCs supported on commercial carbon.

Samples	noble metals precursors		p-block element precursors	
	Type	Dosage (mmol)	Type	Dosage (mmol)
Ru_3Sn_7/C	$RuCl_3 \cdot xH_2O$	0.03		0.07
AuSn/C	$HAuCl_4 \cdot 3H_2O$	0.05	$SnCl_2 \cdot 2H_2O$	0.05
Ag_3Sn/C	$AgNO_3$	0.075		0.025
$RuIn_3/C$	$RuCl_3 \cdot xH_2O$	0.025		0.075
$IrIn_2/C$	$IrCl_3 \cdot xH_2O$	0.03		0.06
Pd_2In/C	K_2PdCl_4	0.06		0.03
Pt_3In/C	$H_2PtCl_6 \cdot 6H_2O$	0.06	$In(NO_3)_3 \cdot xH_2O$	0.02
$Au_{10}In_3/C$	$HAuCl_4 \cdot 3H_2O$	0.1		0.03
Au_3In/C	$HAuCl_4 \cdot 3H_2O$	0.06		0.02

Table S4. The lattice parameters of the samples determined by the Rietveld refinement analysis. And the theoretical values from Inorganic Crystal Structure Database (ICSD) are also provided.

Samples	Space group	a (Å)	b (Å)	c (Å)	α	β	γ
Ru_3Sn_7/C	$Im\bar{3}m$	9.363	9.363	9.363	90°	90°	90°
AuSn/C	$P6_3/mmc$	4.320	4.320	5.521	90°	90°	120°
Ag_3Sn/C	*pmmn*	5.946	4.784	5.180	90°	90°	90°
$RuIn_3$/C	$P4_2/mnm$	7.006	7.006	7.263	90°	90°	90°
$IrIn_2$/C	*Fddd*	9.804	5.352	18.089	90°	90°	90°
Pd_2In/C	*pnma*	5.619	4.216	8.233	90°	90°	90°
Pt_3In/C	$Pm\bar{3}m$	4.028	4.028	4.028	90°	90°	90°
$Au_{10}In_3$/C	$P6_3/m$	10.520	10.520	4.789	90°	90°	120°
Au_3In/C	*pmmn*	5.851	4.737	5.145	90°	90°	90°

Table S5. Comparisons of the electrocatalytic HER performance of Ir_3Sn_7/C with the Ir-based electrocatalysts reported previously.

Catalysts	Electrolyte	Overpotential at 10 mA cm^{-2} for HER (mV)	Tafel slope (mV dec^{-1})	References
Ir_3Sn_7/C	1.0 M KOH	22	27.6	This work
Ir-$Ni(OH)_2$/NF	1.0 M KOH	23	N/A	*ACS Nano* **2025**, 19, 38849
Ir-V_2O_3	1.0 M KOH	26	37	*Angew. Chem. Int. Ed.* **2024**, 26, e202406427
Ir/$NiPS_3$	1.0 M KOH	23	N/A	*Nat. Commun.* **2024**, 15, 2851
Ir-rEGO	1.0 M KOH	114	N/A	*Adv. Funct. Mater*. **2024**, 34, 2313530
Ir/WOx/rGO	1.0 M KOH	53	N/A	*Energy Environ. Mater.* **2021**, 4, 681
IrGa/N-rGO	1.0 M KOH	22	30.2	*Adv. Energy Mater.* **2023**, 13, 2202703
$Ir_{1-X}Rh_xSb$	1.0 M KOH	22	47.6	*Adv. Energy Mater.* **2022**, 12, 2200855.
CBC-Ir	1.0 M KOH	33	16.7	*Adv. Funct. Mater.* **2021**, 31, 2105562
Ni@IrNi	1.0 M KOH	33	32	*Energy Environ. Sci.* **2023**, 16, 6120
Ir/C-800	1.0 M KOH	28	56.2	*ACS Nano* **2023**, 17, 24395
D-$IrTe_2$ HNSs	1.0 M KOH	54	32.7	*Adv. Funct. Mater.* **2020**, 30, 2004375
IrSi	1.0 M KOH	38	N/A	*ACS Catal.* **2022**, 12, 2623
IrP_2@NC	1.0 M KOH	28	50	*Energy Environ. Sci.* **2019**, 12, 952
Ir-gCN	1.0 M KOH	60.2	47.6	*Appl. Catal. B Environ.* **2022**, 310, 121318
Ir-NSs	1.0 M KOH	50	45.4	*Natl. Sci. Rev*. **2020**, 7, 1340

N/A: Not available.

Table S6. Comparisons of the electrocatalytic OER performance of Ir_3Sn_7/C with the Ir-based electrocatalysts reported previously.

Catalysts	Electrolyte	Overpotential at 10 mA cm^{-2} for OER (mV)	Tafel slope (mV dec^{-1})	References
Ir_3Sn_7/C	1.0 M KOH	232	58.8	This work
Ir-rEGO	1.0 M KOH	294	N/A	*Adv. Funct. Mater.* **2024**, 34, 2313530
Ir/$NiPS_3$	1.0 M KOH	236	N/A	*Nat. Commun.* **2024**, 15, 2851
$IrIn_2$/C	1.0 M KOH	267	40.1	*Adv. Funct. Mater.* **2024**, 34, 2311683
IrGa/N-rGO	1.0 M KOH	258	46.7	*Adv. Energy Mater.* **2023**, 13, 2202703
Ir-NSs	1.0 M KOH	266	29.1	*Natl. Sci. Rev.* **2020**, 7, 1340
Ir1/CoOOH	1.0 M KOH	320	33	*J. Am. Chem. Soc.* **2022**, 144, 9271
Ir_1@Co/NC	1.0 M KOH	260	N/A	*Angew. Chem. Int. Ed.* **2019**, 58, 11868
Ir_1-$Ni(OH)_2$	1.0 M KOH	260	78	*Nano Lett.* **2022**, 22, 3832
BPIr_be	1.0 M KOH	290	91	*Adv. Mater.* **2021**, 33, 2104638.
Li-$IrSe_2$	1.0 M KOH	270	N/A	*Angew. Chem. Int. Ed.* **2019**, 58, 14764
$Ir_{0.71}Cu_{0.29}$	1.0 M KOH	355	N/A	*Angew. Chem. Int. Ed.* **2018**, 57, 4505
ex -Ir - $Ni(OH)_2$	1.0 M KOH	270	45.2	*ACS Catal.* **2021**, 11, 5386
$RuIrO_x$	1.0 M KOH	250	50	*Nat. Commun.* **2019**, 10, 4875
Ir-NR/C	1.0 M KOH	296	81.5	*Appl. Catal. B Environ.* **2020**, 279, 119394

Table S7. Comparison of overall water splitting performance of Ir_3Sn_7/C with Ir-based electrocatalysts reported previously in alkaline solution.

Catalysts	Electrolyte	Voltage (V)	References
Ir_3Sn_7/C	1.0 M KOH	1.48	This work
Ir-$Ni(OH)_2$/NF	1.0 M KOH	1.48	*ACS Nano* **2025**, 19, 38849
Ir/$NiPS_3$	1.0 M KOH	1.51	*Nat. Commun.* **2024**, 15, 2851
Ir-rEGO	1.0 M KOH	1.50	*Adv. Funct. Mater*. **202**4, 34, 2313530
$IrIn_2$/C	1.0 M KOH	1.53	*Adv. Funct. Mater.* **2024**, 34, 2311683
IrGa/N-rGO	1.0 M KOH	1.51	*Adv. Energy Mater.* **2023**, 13, 2202703
Ir-NSs	1.0 M KOH	1.575	*Natl. Sci. Rev.* **2020**, 7, 1340
Ir_1@Co/NC	1.0 M KOH	1.60	*Angew. Chem. Int. Ed.* **2019**, 58, 11868
D-$IrTe_2$	1.0 M KOH	1.56	*Adv. Funct. Mater.* **2020**, 30, 2004375
BP-Ir	1.0 M KOH	1.54	*Adv. Mater.* **2021**, 33, 2104638
Li-IrSe	1.0 M KOH	1.48	*Angew. Chem. Int. Ed.* **2019**, 58, 14764
d-$ZnIr(OH)_6$ NSs/C	1.0 M KOH	1.48	*Energy Environ. Sci.* **2022**, 15, 1672
Ir/MoS_2	1.0 M KOH	1.57	*ACS Energy Lett.* **2019**, 4, 368
$RuIrO_x$	1.0 M KOH	1.47	*Nat. Commun.* **2019**, 10, 4875
Ir-NR/C	1.0 M KOH	1.57	*Appl. Catal. B Environ.* **2020**, 279, 119394
NiVIr-LDH	1.0 M KOH	1.52	*Nat. Commun.* **2019**, 10, 3899

Table S8. Concentrations of Ir and Sn ions leached from the Ir_3Sn_7/C catalyst into the electrolyte over 140 h of overall water splitting.

Elements	Sn	Ir
Concentrations (ppb)	2.8	1.0

Table S9. Comparison of AEM water electrolyzer performance of Ir_3Sn_7/C with those of recently reported electrocatalysts.

Catalysts	Cell voltage (V)	Stability test (h)	Testing condition	References
Ir_3Sn_7/C||Ir_3Sn_7/C	1.77@1 A cm^{-2}	200@1 A cm^{-2}	1.0 M KOH, 50 °C	This work
Ni_3S_2/Cr_2S_3@NF||Ni FeCr-LDH@NF	2.04@1 A cm^{-2}	35@1 A cm^{-2}	1.0 M KOH, 60 °C	*J. Am. Chem. Soc.* **2022**, 144, 6028
Pt_1/CoHPO||Ti felt	1.8@1 A cm^{-2}	100@1 A cm^{-2}	0.1 M KOH, 80 °C	*Nat. Commun.* **2022**, 13, 3822
d-(Fe,Ni)OOH|| NiMoN	1.55@500 mA cm^{-2}	200@375 mA cm^{-2}	6 M KOH, 60 °C	*Adv. Mater.* **2023**, 35, 2306097
MoO_2@Ru||NiFe LDH@NF	1.78@1 A cm^{-2}	200@1 A cm^{-2}	1.0 M KOH, 50 °C	*Adv. Energy Mater.* **2023**, 2301492
Ni_3N/Ni||$NiFe_2O_4$	1.88@500 mA cm^{-2}	24@500 mA cm^{-2}	1.0 M KOH, 55 °C	*Energy Environ. Sci.* **2022**, 15, 185
(Ni, Fe)$_3S_2$/NFF|| (Ni, Fe)$_3S_2$/NFF	1.90@300 mA cm^{-2}	400@400 mA cm^{-2}	0.5 M KOH	*Adv. Funct. Mater.* **2024**, 2400979
Ir@Zr-CoP||NiFe-LDH	1.88@1 A cm^{-2}	150@1 A cm^{-2}	1.0 M KOH	*Adv. Energy Mater.* **2023**, 13, 2301841
PtPd-HEA||NiFe-LDH	1.81@1 A cm^{-2}	100@1 A cm^{-2}	1.0 M KOH, 80 °C	*ACS Catal.* **2025**, 15, 11022
Pt SACs-$NiCrO_3$/NF||$NiFeO_x$ H_y/NF	1.51@100 mA cm^{-2}	100@100 mA cm^{-2}	1.0 M KOH	*Adv. Funct. Mater.* **2025**, 35, 2416678
JH-Pt_2Tb/C||NiFe-LDH	1.79 V@1 A cm^{-2}	100@1 A cm^{-2}	1.0 M KOH, 80 °C	*Adv. Mater.* **2025**, 37, 2506936
Ru As/WCx‖NiFeOHx-NF	1.79@1 A cm^{-2}	190@1 A cm^{-2}	1.0 M KOH, 80 °C	*J. Am. Chem. Soc.* **2024**, 146, 4883
Pt_{SA}–Mn||Fe–Ni LDHs	1.97@1 A cm^{-2}	600@500 mA cm^{-2}	1.0 M KOH, 60 °C	*ACS Nano* **2024**, 18, 16222
Ni_3Mo||Ni–FeLDH	1.82@1 A cm^{-2}	48@1 A cm^{-2}	1.0 M KOH	*ACS Catal.* **2023**, 13, 11589
UP-RuNiSAs/C|| $NiFeO_x$	1.95@1 A cm^{-2}	250@1.0 A cm^{-2}	1.0 M KOH, 70 °C	*Nat. Commun.* **2024**, 15, 2218
P-Os/NiFe|| RuO_2/NiFe	2.02 V@1 A cm^{-2}	500@100 mA cm^{-2}	1.0 M KOH, 60 °C	*Adv. Funct. Mater.* **2024**, 34, 2408517

Table S10. Comparison of PEM water electrolyzer performance of Ir_3Sn_7/C with those of recently reported electrocatalysts.

Catalysts	Cell voltage (V)	Stability test (h)	Testing condition	References
Ir_3Sn_7/C||Ir_3Sn_7/C	1.82@1 A cm^{-2}	100@500 mA cm^{-2}	0.5 M H_2SO_4	This work
Ni-RuO_2||Pt/C	1.95@1 A cm^{-2}	1000@200 mA cm^{-2}	0.5 M H_2SO_4	*Nat. Mater.* **2023**, 22, 100
RuFe/CF||Pt/C	1.898@1 A cm^{-2}	250@200 mA cm^{-2}	0.5 M H_2SO_4	*Adv. Mater.* **2024**, 36, 2312369
Ir_3Ni NCs/C||Ir_3Ni NCs/C	1.77@0.5 A cm^{-2}	190@100 mA cm^{-2}	0.2 M $HClO_4$	*J. Am. Chem. Soc.* **2024**, 146, 7858
Pt/C||IrO_2	2.43@1 A cm^{-2}	-	0.5 M H_2SO_4	*Adv. Mater.* **2025**, 37, 2420159
RuMnFeMoCo@CF||Pt/C	1.85@1 A cm^{-2}	150@500 mA cm^{-2}	0.5 M H_2SO_4	*Angew. Chem. Int. Ed.* **2025**, 64, e202503330
La-RuO_2||Pt/C	1.82@1 A cm^{-2}	120@100 mA cm^{-2}	0.5 M H_2SO_4	*Angew. Chem. Int. Ed.* **2025**, 64, e202425569
RuO_2-com||Pt/C	1.82@1 A cm^{-2}	75@500 mA cm^{-2}	0.5 M H_2SO_4	*ACS Nano* **2025**, 19, 8773
TS-Ir/MnO_2||Pt/Ti	1.75@500 mA cm^{-2}	200@500 mA cm^{-2}	0.2 M $HClO_4$	*Nat. Commun.* **2024**, 15, 95
Ir@Sr-p-TiO_2||Ir@Sr-p-TiO_2	1.8@20 mA cm^{-2}	150@20 mA cm^{-2}	0.5 M H_2SO_4	*Adv. Energy Mater.* **2024**, 14, 2303987
PtRu-Co_3O_4||Pt/C	1.83@1 A cm^{-2}	200@200 mA cm^{-2}	0.5 M H_2SO_4	*J. Am. Chem. Soc.* **2024**, 146, 28728
$NdMn_{1.5}Ru_{0.5}O$||Pt/C	1.97@500 mA cm^{-2}	100@500 mA cm^{-2}	0.5 M H_2SO_4	*J. Power Sources* **2024**, 604, 234416
Co_3O_4/MnO_2||Pt/C	1.638@100 mA cm^{-2}	-	0.5 M H_2SO_4	*Energy Environ. Sci.* **2024**, 17, 5972
RuO_2-com||Pt/C	2.15@1 A cm^{-2}	-	0.5 M H_2SO_4	*Nat. Commun.* **2025**, 16, 337
M-RuIrFeCoNiO_2||Pt/C	1.85@1 A cm^{-2}	500@1 A cm^{-2}	0.5 M H_2SO_4	*Sci. Adv.* **2023**, 9, eadf9144

1. G. Kresse and J. Furthmüller, *Phys. Rev. B*, 1996, **54**, 11169-11186.
2. G. Kresse and J. Hafner, *Phys. Rev. B*, 1993, **47**, 558-561.
3. B. Hammer, L. B. Hansen and J. K. Nørskov, *Phys. Rev. B*, 1999, **59**, 7413-7421.
4. J. P. Perdew, K. Burke and M. Ernzerhof, *Phys. Rev. Lett.*, 1996, **77**, 3865-3868.
5. P. E. Blochl, *Phys. Rev. B* 1994, **50**, 17953-17979.
6. J. Klimeš, D. R. Bowler and A. Michaelides, *Phys. Rev. B* 2011, **83**, 195131.
7. S. Grimme, J. Antony, S. Ehrlich and H. Krieg, *J. Chem. Phys.*, 2010, **132**, 154104.
8. L.-P. Ji, F. Yi, C.-Q. Cheng, Z. Li, W. Guan, B. He, Z. Liu, J. Mao, S.-J. Zheng, C.-K. Dong, Y.-Y. Zhang, H. Liu, L. Cui and X.-W. Du, *Small*, 2022, **18**, 2107481.